DEVELOPMENT OF TOOLS NEEDED FOR RADIATION ANALYSIS OF A CUBESAT DEPLOYER USING OLTARIS

A Thesis

presented to

the Faculty of California Polytechnic State University,

San Luis Obispo

In Partial Fulfillment

of the Requirements for the Degree

Master of Science in Aerospace Engineering

by

MaryCarmen Gonzalez-Dorbecker

August 2015

COMMITTEE MEMBERSHIP

TITLE:	Development of Tools Needed for Radiation Analysis of a CubeSat Deployer Using OLTARIS
AUTHOR:	MaryCarmen Gonzalez-Dorbecker
DATE SUBMITTED:	August 2015
COMMITTEE CHAIR:	Dr. Kira Abercromby, Ph.D. Associate Professor of Aerospace Engineering
COMMITTEE MEMBER:	Dr. Jordi Puig-Suari, Ph.D. Professor of Aerospace Engineering
COMMITTEE MEMBER:	Dr. Eric Mehiel, Ph.D. Professor/Department Chair of Aerospace Engineering
COMMITTEE MEMBER:	Max Glicklin, M.S. Research Scientist at Lockheed Martin

ABSTRACT

Development of Tools Needed for Radiation Analysis of a CubeSat Deployer Using OLTARIS

MaryCarmen Gonzalez-Dorbecker

Currently, the CubeSat spacecraft is predominantly used for missions at Low-Earth Orbit (LEO). There are various limitations to expanding past that range, one of the major ones being the lack of sufficient radiation shielding on the Poly-Picosatellite Orbital Deployer (P-POD). The P-POD attaches to a launch vehicle transporting a primary spacecraft and takes the CubeSats out into their orbit. As the demand for interplanetary exploration grows, there is an equal increase in interest in sending CubeSats further out past their current regime. In a collaboration with NASA's Jet Propulsion Laboratory (JPL), students from the Cal Poly CubeSat program worked on a preliminary design of an interplanetary CubeSat deployer, the Poly-Picosatellite Deep Space Deployer (PDSD). Radiation concerns were mitigated in a very basic manner, by simply increasing the thickness of the deployer wall panels. While this provided a preliminary idea for improved radiation shielding, full analysis was not conducted to determine what changes to the current P-POD are necessary to make it sufficiently radiation hardened for interplanetary travel.

This thesis develops a tool that can be used to further analyze the radiation environment concerns that come up with interplanetary travel. This tool is the connection

between any geometry modeled in CAD software and the radiation tool OLTARIS (On-Line Tool for the Assessment of Radiation In Space). It reads in the CAD file and converts it into MATLAB, at which point it can then perform ray-tracing analysis to get a thickness distribution at any user-defined target points. This thickness distribution file is uploaded to OLTARIS for radiation analysis of the user geometry.

To demonstrate the effectiveness of the tool, the radiation environment that a CubeSat sees inside of the current P-POD is characterized to create a radiation map that CubeSat developers can use to better design their satellites. Cases were run to determine the radiation in a low altitude orbit compared to a high altitude orbit, as well as a Europa mission. For the LEO trajectory, doses were seen at levels of 10^2 mGy, while the GEO trajectory showed results at one order of magnitude lower. Electronics inside the P-POD can survive these doses with the current design, confirming that Earth orbits are safe for CubeSats. The Europa- Jovian Tour mission showed results on a higher scale of 10^7 mGy, which is too high for electronics in the P-POD. Additional cases at double the original thickness and 100 times the original thickness resulted in dose levels at orders of about 10^7 and 10^4 mGy respectively. This gives a scale to work off for a "worst case" scenario and provides a path forward to modifying the shielding on deployers for interplanetary missions. Further analysis is required since increasing the existing P-POD thickness by 100 times is unfeasible from both size and mass perspectives. Ultimately, the end result is that the current P-POD standard does not work too far outside of Earth orbits. Radiation-based changes in the design, materials, and overall shielding of the P-POD need to be made before CubeSats can feasibly perform interplanetary missions.

Keywords: Radiation, OLTARIS, P-POD, GCR, SPE, Interplanetary, Cal Poly, CubeSat, PolySat, Ray-Tracing

ACKNOWLEDGMENTS

I want to thank my professors, peers, and everyone that helped me during this process. Especially Dr. A for having faith in me and letting me go through with this project. Also, thanks to my mom for texting me every day spring quarter asking if I was done yet, Rob for asking if I had updates to my code so he could use it, my kitten for sitting on my computer every time I tried to type and delaying me for a few days, and Liam for putting up with me and keeping me from going completely crazy.

TABLE OF CONTENTS

LIST OF TABLES

LIST OF FIGURES

CHAPTER 1

Introduction

Introduction to Project Concept

Background

The CubeSat form factor was created in 1999 by Dr. Jordi Puig-Suari from California Polytechnic State University and Dr. Bob Twiggs from Stanford University[1].The standard 1U CubeSat with dimensions of 10 x 10 x 10 cm^3 was developed to be a low-cost satellite for students to design, build, launch, and operate all the way through to the satellite's end of life. A short development time and ride-sharing capability makes these picosatellite missions possible. Today, the CubeSat standard is used not only by students but also by professionals at both small companies and large corporations. The capabilities have improved greatly, and scientists and engineers are looking toward the next step: interplanetary travel.

Before proceeding with interplanetary missions, however, there are currently some limitations that need to be addressed. One such concern is that CubeSats are designed predominantly for Low-Earth Orbit (LEO) missions. To extend this range, limitations such as a lack of sufficient radiation shielding on the Poly-Picosatellite Orbital Deployer (P-POD) need to be analyzed.

Overview

The scope of this thesis is to look at the existing model of the P-POD and develop a radiation analysis method to use on the structure. Currently, no in-depth radiation analysis has been conducted, and this is a big step that needs to be completed for design improvement. This information can then be carried over into radiation analysis on the preliminary deployer design for interplanetary CubeSat missions as well as on CubeSats themselves. The goal at the end of this thesis is to map the radiation environment inside the P-POD from the data analyzed so that CubeSat developers know how best to design their satellites and where to avoid putting their sensitive electronics. It will also provide key information for making the transition to interplanetary CubeSat missions.

Poly-Picosatellite Deep Space Deployer (PDSD)

The current deployer design, the P-POD, is a jack-in-the-box-style deployer that contains the CubeSats as they are launched into space. It attaches to the launch vehicle and carries the CubeSats out into orbit, deploying them once the primary mission is completed. It serves the dual purpose of protecting the CubeSats until they reach the start of their mission and protecting the primary spacecraft from the CubeSats.

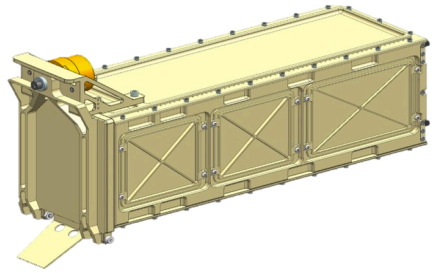

Figure 1. Design of the Mk. IV P-POD [1].

The P-POD, shown in Figure 1, has a standard size capable of containing 3U, meaning that its internal dimensions are about 10 x 10 x 30 cm^3. This allows for it to contain three 1U CubeSats, a 1U and a 2U, or one large 3U CubeSat. There are 0.5U and 1.5U CubeSats as well, but these are less common. However, any combination that adds up to 3U will fit inside the P-POD.

The Poly-Picosatellite Deep Space Deployer (PDSD) is a concept that arose from a collaboration between Cal Poly and NASA's Jet Propulsion Laboratory (JPL) to create a design for an interplanetary CubeSat deployer. This new design aimed to address the concerns with interplanetary CubeSat travel that are not currently addressed with the P-POD design[1]. This concept can be seen in Figure 2. Radiation concerns were mostly ignored and only the basic mitigation strategy of arbitrarily increasing panel thickness was used. While this can improve radiation shielding, full analysis was not conducted to determine what changes to the current P-POD are necessary to make it sufficiently radiation hardened for interplanetary travel.

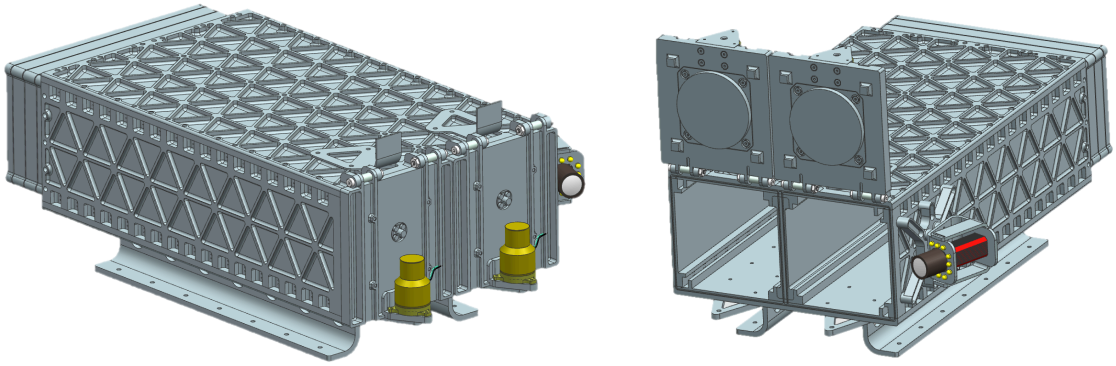

Figure 2. Design of the PDSD [1].

The PDSD design is very similar to that of the P-POD. One of the biggest changes is the increase in size from a 3U to a 6U deployer. This means the internal dimensions are about 10 x 20 x 30 cm^3. A CubeSat going on an interplanetary mission requires a lot more power and shielding, therefore requiring a larger deployer. The PDSD has the capability to contain any combination of CubeSats that add up to 6U, including a 6U CubeSat. Its doors can open together in this case, and the middle divider would be removed. In the case of using two 3U CubeSats, the options are there for deploying at the same time or at separate times. This means that the P-POD is a good substitute for simulations since its only difference are dimensions. There are a few other differences as well, but none that affect radiation shielding of the deployer, such as the wall panel general design, which does not include access ports. The deployer mounting method is also different; standoffs keep the PDSD off the surface of the primary satellite rather than directly on it. The door opens with two pin pullers rather than a Non-Explosive Actuator (NEA).

The reason the P-POD is used instead of the PDSD is because there are established pre-existing CAD files ready to use in developing a radiation method. This eliminates additional time required to fine-tuning the PDSD CAD models that are still subject to changes.

Project Relevance

This project is an important concept because as previously mentioned, there is no thorough radiation analysis that has been done on either the current P-POD or the conceptual PDSD. Radiation tends to be ignored because it is a difficult environment and the analysis is not easy. However, this information is vital in improving the capability of both the deployers and the CubeSats they contain. Knowledge of the radiation environment that CubeSats see inside deployers will help developers better design and shield their CubeSats, as well as leading to the next step in taking CubeSats interplanetary. It is also important in maintaining the ride-sharing capabilities and affordability that CubeSats have now. A simple solution to radiation problems is to increase the thickness of the satellite walls, but on a scale this small, it is not practical to add mass and weight. CubeSats were not designed to be primary spacecraft; to keep them as secondary payloads, they are restricted on power and weight limits. More analysis needs to be performed to understand what is necessary and what can be done besides drastically increasing wall panel thickness.

Thesis Overview

In this thesis document, a background on radiation and the radiation environment in space is covered, as well as general information on radiation transport methods through materials. A detailed explanation of the radiation analysis tool used for this project is provided, including the options the program has, the methodology it uses, and the verification of its results.

The next section after that talks about the process for preparing the P-POD (or any other) geometry for radiation analysis, and the steps taken to create the files that the radiation analysis tool, OLTARIS, uses. This includes an overview of the format required for the files as well as a few of the problems encountered along the way.

The last main section of this document discusses the output received from OLTARIS and the procedure for analyzing this data. The results are presented, elaborated on, and conclusions are stated.

Background on Radiation

General Information

The radiation environment is particularly volatile and harmful to spacecraft. Depending on the type and intensity, radiation degrades spacecraft components over time or can cause a quick and sudden death due to electronics malfunctioning. Radiation is considered to be composed of energetic particles and photons, and has the ability to pass through materials, affecting not only the external layers of objects but the interiors as

well. In space, three naturally occurring sources of radiation are responsible for spacecraft damage: the trapped radiation belts, galactic cosmic rays, and solar particle events [8,18].

Radiation Belts

The strength of Earth's magnetic field has resulted in concentrations of trapped energetic particles. These electrons and protons follow the magnetic field lines and are the result of high-energy collisions between cosmic rays and Earth's atmosphere. The particles become trapped through a process called "magnetic mirroring," in which charged particles try to move toward a region of higher magnetic field strength but are pushed back and end up stuck in a region of weak magnetic field strength. Although the belts are relatively "static" in nature, they vary slightly based on changes in the magnetic field and solar events [8, 18].

There are two main belts. The first belt (Inner Belt) ranges in altitude from approximately 1000 to 3000 km above Earth's surface and is composed of electrons and protons [8, 18]. It also contains a region known as the South Atlantic Anomaly, which is where the belt dips down and is the closest to Earth's surface. At this height of about 200 km, it poses a higher radiation does than would otherwise be expected so close to the surface. This region is caused by the offset that occurs between Earth's spin axis and its magnetic poles. The second belt (Outer Belt) ranges in altitude from about 13,000 to 60,000 km above Earth's surface, and is composed of mostly electrons [8, 18].

More recently, two spacecraft were sent to observe and take data of the belt regions and the magnetic activity there. Data from these Van Allen probes revealed the existence of a third belt that was formed shortly after solar activity caused the first two belts to swell in size[19]. Very high energy particles from this event moved past the two belts and settled into a thinner, outer belt, where the particles behaved differently than the particles in the first two belts. This region was wiped out in the same way it was formed, during a solar storm event a few weeks after its creation. Though it didn't stay for long, this third belt shows that there is still a lot to learn about these regions of trapped radiation.

Galactic Cosmic Rays

Galactic cosmic rays, or GCRs, are very high-energy particles that originate outside of the solar system. They are mostly atomic nuclei with no electrons that are trapped in the galactic magnetic sphere. They are present in higher rates during solar minimum and lower rates during solar maximum [8,18]. Their behavior is more difficult to predict and their total dose effect isn't usually very high due to the unlikelihood of actually being hit by many, but their biggest effect on electronics is to cause single event changes, which will be explained in a subsequent section.

Solar Particle Events

Solar Particle Events, or SPEs, are the result of solar activity. The Sun periodically releases particles, mostly protons, in coronal mass ejections (CME) and solar flares. During these events, the particles cause an increase in the flux density of energetic

particles throughout the solar system. CME events are hard to predict or model, and can last anywhere from a few hours to a few weeks [8,18]. Solar flares are the flash of light that often accompany a CME and can accelerate particles toward Earth. They last a few minutes to a few hours [4]. Table 1 shows the different classes of solar flare events and their intensities. On average, SPEs are not very intense and the particles are blocked by Earth's magnetic field, as demonstrated in Figure 3. On occasion, there are isolated large events that can result in higher levels of damage. SPEs follow the Sun's activity cycle, and can occur as often as multiple times per day during solar maximum, while only occurring about once a week during solar minimum [25].

Table 1. Table of Solar Flare Classifications [16].

Class	Intensity in erg/cm^{2}s (MeV/ cm^{2}s)
B	10^{-4} (624.15)
C	10^{-3} (6241.51)
M	10^{-2} (62415.10)
X	10^{-1} (624151)

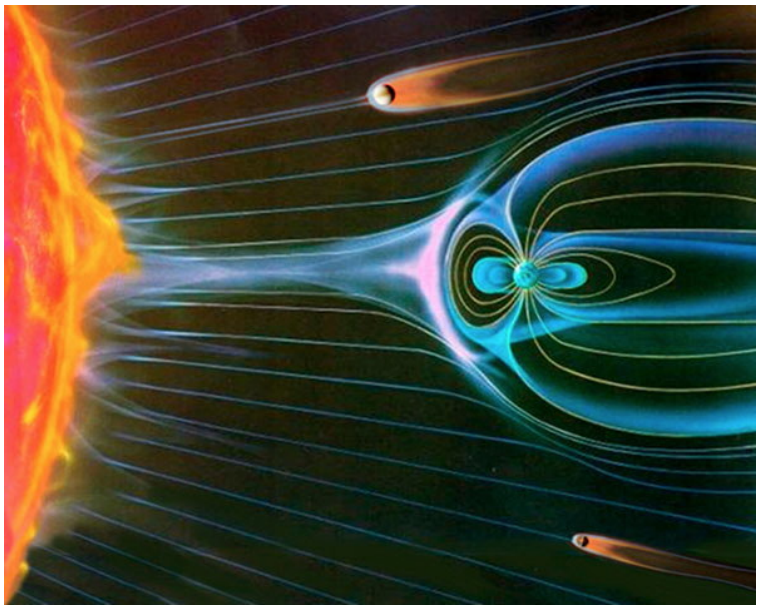

Figure 3. Depiction of Earth's Magnetic Field Blocking Solar Particles [9].

Radiation Effects on Electronics

Radiation causes changes to electronics that can result in temporary or permanent damage. These changes are based on the type of radiation the electronic component is exposed to and the way in which the radiation interacted with the electronic component.

Displacement Damage

In displacement damage, the behavior of the electronic is altered, but there is a chance that it will return to normal. Electronic materials rely on their lattice structure to transport a current and function properly. When a high-energy radiation particle hits this lattice, it can dislodge or displace the nucleus of the atom at the point where it collided. The energy from this could spread to create more displacements that further affect the structure. This prevents the electronic from properly transporting a current or functioning

the way it needs to [18]. In some cases, after the collisions have stopped, the displaced nuclei are able to move back and fill the vacant spots, re-creating the original lattice structure and returning to a lower energy state. Of course, even if this is the case there is no guarantee that every nucleus will return to its vacated spot; some defects might still remain.

Single Event Effects

Single Event Effects (SEE) are the result of radiation ionizing the matter that it hit[8,18]. This means that electrons are pushed into the conduction band, creating small energy spikes. These spikes can cause disruptions in electronic components. The three main categories of disruptions are single event upset, single event latchup, and single event burnout.

Single Event Upset

Single Event Upsets (SEU) are a type of soft error that results in a bit flip. This means the affected electronic device can continue to function normally, with the only concern being corrupted data stored in the flipped bit. Software exists to detect and correct these upsets so that the effects can be reduced [8,18].

Single Event Latchup

A Single Event Latchup (SEL) is a slightly more serious concern if not kept in check. A short circuit is formed between the power source and ground, and if the power is left unchecked large currents occur that can cause failure to the device [8,18]. SELs are

usually fixed by software monitoring for power changes that then turns the circuit power off and then back on again.

Single Event Burnout

Single Event Burnout (SEB) occurs when radiation causes excessive power draw and a high current. This increased current burns out the device because the breakdown voltage of the material is exceeded. This happens in particular to power metal oxide semiconductor field effect transistors (MOSFETs), which are common in CubeSats. SEBs result in permanent failure to the affected electronic device [8,18].

Transportation Model Selection

The tool used to perform radiation analysis for this thesis, OLTARIS (On-Line Tool for the Assessment of Radiation in Space), is a web-based tool created by NASA's Langley Research Center. More detail will be given on the background and verification for OLTARIS in a later section, but its options in regards to the way the radiation environment is selected are described here.

Environments

OLTARIS allows the user to select the environment that the radiation analysis will be performed in. These environments include focuses on GCRs, SPEs, Earth Orbits, and Europa. Within these environments there are further categories that can be selected[14]. Figure 4 shows the environment selection drop-down menu.

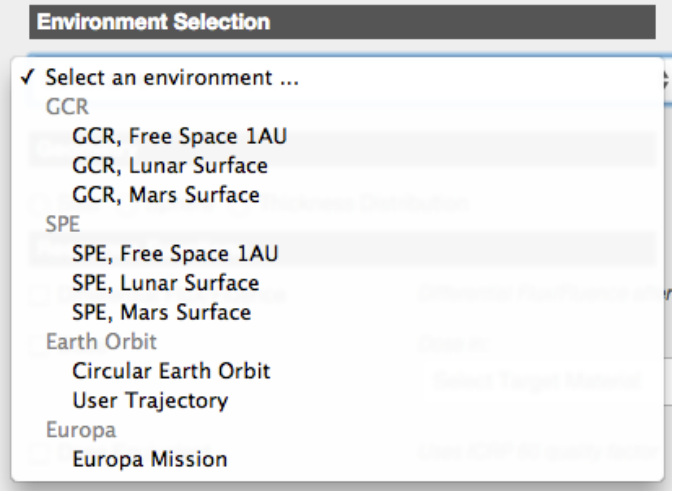

Figure 4. Environment Selection Menu [13].

GCR

The GCR environment allows the user to select "Free Space 1AU", "Lunar Surface", or "Mars Surface." This means that the GCR radiation effects are measured at these three locations. Within each option, there are further selections that can be made. The first is "Select Historical Solar Min/Max," which allows the user to pick solar minimum or maximum at one of the historical dates on record and then set a mission duration at that time. The second option says "Enter Date," and allows the user to enter either start and end dates, or a start date and a mission duration. The last option is the "Enter Solar Modulation Parameter," in which the user can enter a parameter value and a mission duration.

SPE

The SPE radiation environment options are the same as for the GCR radiation: Free Space 1AU, Lunar Surface, and Mars Surface. Once one of these locations is

selected, the user has two further options. The first is “Historical SPE,” where the user is presented with a list of historical SPE events with multiplication factors set a default value of 1.0. The user can select any combination of one or several events and can also change the multiplication factors for these events to increase or decrease the effects of that event. The effects are added when multiple dates are selected. The second option, “User Defined SPE,” results in four more options: Weibull, Exponential in Energy, Exponential in Rigidity, or Band Function. These are all curve fits that when selected display the equation used and allow the user to input the parameters needed.

Earth Orbit

The Earth Orbit environment has two options: Circular and User Trajectory. In the “Circular” option, the user enters mission start and end dates or a start date and mission duration (in days), an altitude (km), and an inclination (deg) for the orbit. There is also an option for selecting the Constellation Program Design Specification for Natural Environments (DSNE), which fixes the dates, altitude, and inclination, but allows the user to change the mission duration. If the “User Trajectory” option is selected, a drop-down menu appears that lets the user choose a trajectory that has been previously created and uploaded by the user. In both cases, the user can select any combination of “GCR,” “Trapped Proton,” and “Neutron Albedo.” Figure 5 shows the Circular Earth Orbit options since these were used for this thesis.

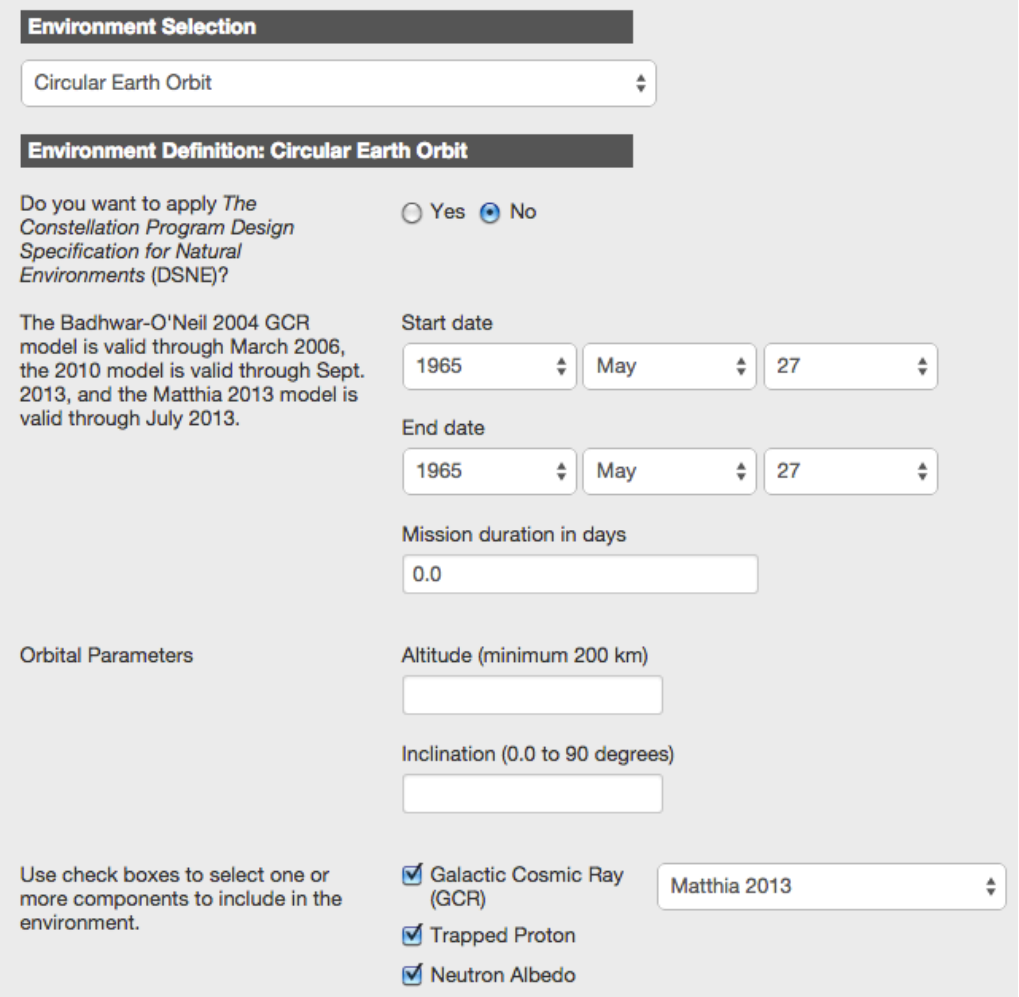

Figure 5. Circular Earth Orbit Selection Menu [13].

Europa

The most recent addition to the OLTARIS environment selections is the "Europa" environment. This option is the design reference environment for a NASA/ESA joint Europa mission[14]. The scenario options are different mission segments: 105 Days at Europa, Jovian Tour, Flux at $5R_j$, and Flux at $9R_j$. In all of these cases, the user then selects any combination of "Trapped Electrons," "Trapped Protons," and "Trapped Heavy-Ions (averaged)." These radiation boundaries are similar to the Earth Orbit

options, but since not all of them are available at all of the environment scenarios given, the boxes may be grayed out depending on the mission segment selected. Figure 6 shows all of the Europa options.

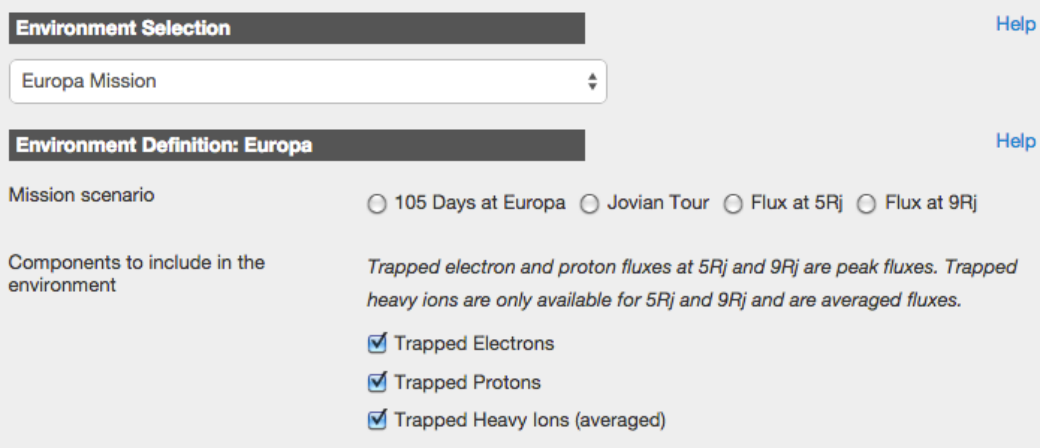

Figure 6. Europa Mission Selection Menu [13].

The Europa options are the closest thing to an interplanetary mission currently available. However, it requires selections of missions that cannot be modified as much as would be desired, leading to less accurate results. OLTARIS is constantly changing, improving, and adding new features. The Europa option is the newest addition and as such, it is still very limited. When OLTARIS increases its capability, the method developed in this thesis can be used to get better results.

Radiation Response Options

Similar to the environment options, OLTARIS has various options for radiation response functions to be evaluated. These options are "Differential Flux/Fluence," "Dose," "Dose Equivalent," "Effective Dose Equivalent," "TLD-100," "TEPC," and

"LET," and can be chosen based on what material the user is analyzing[14]. The user can select all of them or only some of them based on their needs. Not all of the response functions (such as TEPC) are available for all of the environments or geometries. The selection layout is shown Figure 7.

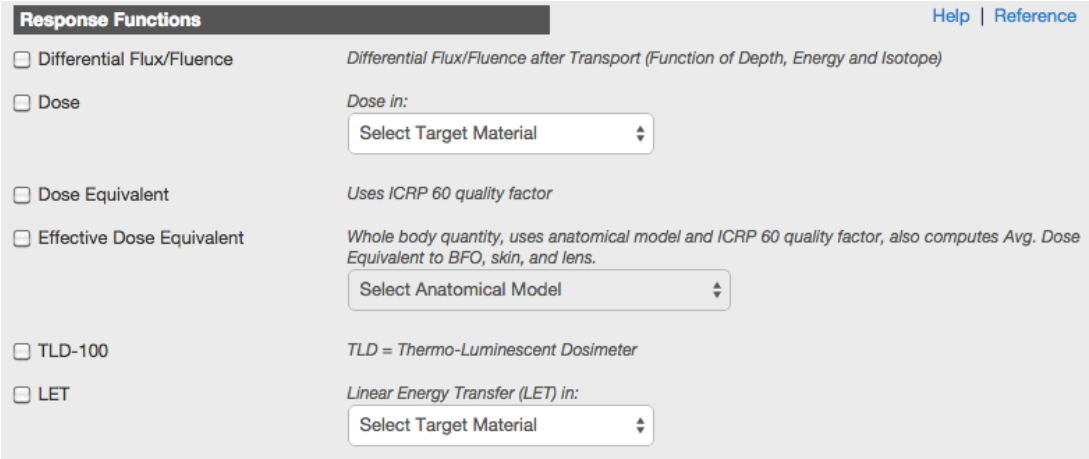

Figure 7. Example of Response Function Selection Section [13].

The details of which functions are used and how each response is found will be explained in a later section. The sub-sections below are to explain to the user what the different options output for results, not how they get the results or other background.

Differential Flux/Fluence

The Differential Flux/Fluence option gives an output based on the transport calculation. The results change based on which type of geometry is used. If a user-created thickness distribution is selected, the output is an array of flux/fluence vs. depth, energy, and isotope. The depth function is done for the spatial grid of each of the materials in the

thickness distribution. When the geometry used in one of the default slab options, the results are only for the grid of the slab.

Dose

The Dose response shows results of dose at a point when using a thickness distribution, where the point is specified in the distribution. Otherwise, the results are of dose vs. depth for each material being used. When this box is selected, a drop-down menu asks the user to select a target material of either organic tissue or silicon.

Linear Energy Transfer (LET)

The LET response option shows differential and integral flux/fluence versus LET and also versus depth at the target point specified in the user thickness distribution. If a slab is used then the results are for the spatial grid of each material. When selected, this option also has a drop-down menu that allows the user to select if the response is being considered for tissue or silicon.

Other Options

OLTARIS has other radiation response options such as “Dose Equivalent,” “Effective Dose Equivalent,” “TLD-100,” and “TEPC.” All of these options are useful in analyzing the radiation effects on human tissue. A human phantom body can be downloaded and added to the chosen thickness distribution to better see these results. Since they were not used in the completion of this thesis, they will not be covered in this

document. For more information, see the documentation page of OLTARIS or look in the resources at the end of this paper.

OLTARIS

General Background

OLTARIS (On-Line Tool for the Assessment of Radiation In Space) is an online radiation analysis tool that outputs results of space radiation on humans and electronics [12]. It uses the HZETRN2005 radiation transport code as its main base for analysis along with the NUCFRG2 code, which are both described in the next section. The interface is designed to meet user needs by allowing users to enter the information in five main categories. These are: Radiation Environment, Material Properties, Geometry, Transport, and Response Functions. The selections within these categories vary on a case-by-case basis. The interface and internal workings of OLTARIS have a modular design, allowing separate parts to be updated without requiring knowledge of any other part. When updates or changes are made, the entire system is re-tested to verify that the system still retains its functionality and accuracy. Figure 8 shows a visual of the OLTARIS program flow and its modular design. Each component is explained or touched upon in the subsequent sections following the figure.

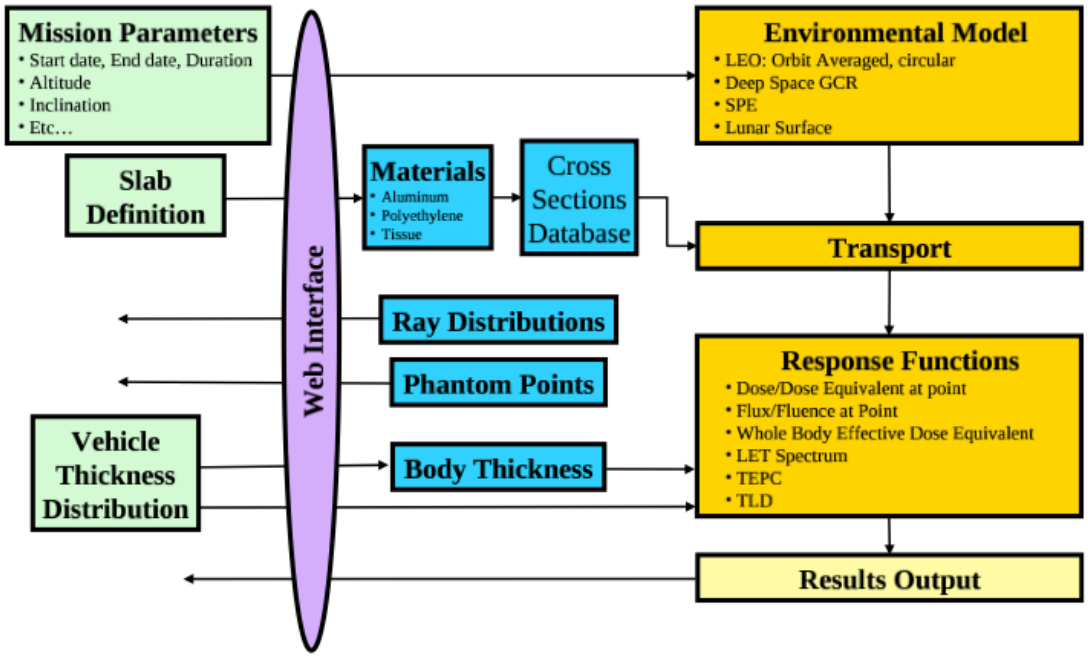

Figure 8. Visual of OLTARIS Program Flow and Design [12].

HZETRN2005 and NUCFRG2

HZETRN stands for High charge (z) and Energy TRaNsport, and is a research-based code designed to perform radiation analysis under various conditions. It analyzes the shielding effectiveness of materials exposed to radiation by giving a solution to the Boltzmann transport equation, which is explained in the "Particle Transport" section [5]. OLTARIS uses this as its base and then expands on it further. Another code, NUCFRG2 is also used. This stands for NUClear FRaGmentation Database and is used by OLTARIS for the heavy ion cross sections. It is a geometric model based on an abrasion-ablation concept in which a piece of nucleus is abraded (sheared off), causing it to form an excited state that ablates (decays) by particle emission [12, 21].

Functionality

In order to use OLTARIS, the user first needs to be approved. OLTARIS is designed to be used by professionals and those in academics that have at least a basic understanding of the radiation environment in space and are using the tool for projects. This is to prevent any people from using it poorly and slowing down the servers for others. More importantly, some of the content on the website is considered part of International Traffic in Arms Regulations (ITAR) and needs to be limited and regulated.

Web Interface

When the user first logs into the site, they are directed to the "Projects" page, which is the first tab and where all of the projects are created and saved. Figure 9 shows the different tab options that are available at the top of every page. A project is the entire grouping of information regarding the environment, mission parameters, thickness distribution, and results for a any specific case. Each of the components can be edited. In conjunction with projects are "Jobs", which are the project cases that have been submitted for analysis. A user can create a project and is led through the steps of filling the settings, and then at the end is given the option to submit the project as a job. When this is done, it will be listed in the Jobs page that can be accessed from the Projects page. The user simply selects the "List" option next to its name in the Projects menu, and then is re-directed to the Jobs page. The Jobs page allows the user to select a specific job and then either view the results, some of which are presented in a table format, or download the results including data and graphs.

Figure 9. Six Available Tabs for Every OLTARIS Page [13].

The next tab option is "Uploads." When this tab is selected, a drop-down menu shows that the user can select "Thickness Distribution" or "Trajectories". When one of the two is selected, the user is directed to an upload page where files can be loaded onto OLTARIS and saved for use with projects and jobs.

The third tab, "Slabs and Spheres", is similar to the "Uploads" tab. When selected, the user then chooses between sphere or slab from a drop-down menu. Then the user is directed to a page where a new sphere or slab can be created. The user selects the material from a list of saved OLTARIS defaults, and then sets the units and a desired thickness.

In the "Materials" tab, the user is directed to a page that lists the default materials included in OLTARIS. There is also an option to add a new material, which can be used when the slab option is chosen for the geometry. If this option selected, the user needs to enter in the material's elemental or molecular mass percentages, or its chemical formula. Then this is submitted and the site will compute the material cross sections for use with a slab.

The last two tabs, "Documentation" and "Logout", are straightforward. The Documentation tab leads the user to a page of links to various resources regarding how to

use OLTARIS, how to upload to the site, how the calculations are performed, etc. The Logout link logs the user out from the site.

Thickness Distributions

One of the main internal components of OLTARIS is the ability to process a thickness distribution uploaded by a user. This allows the user to model their own vehicle rather than attempting to recreate it in parts with slabs and spheres. The options require the user to download a ray distribution, rotated or un-rotated, and then perform a ray-tracing process to find the thickness of the vehicle geometry along each ray. The OLTARIS distributions are of 42, 492, 512, 968, 1002, 4002, 9002, and 10000 rays. The "target point" is the start point of the rays. This means that each job finds the radiation levels at one point in the vehicle geometry. Multiple jobs within one project are necessary to understand the entire vehicle. For effective dose calculations, OLTARIS provides human body phantom thickness distributions for download that can be combined with the vehicle geometry. This allows the user to analyze the radiation in the body at a specific orientation relative to their vehicle. In this case, there are three points used for orientation of the body and then five target points corresponding with body zones to be used separately for calculation of the dose at each one. Further detail will be provided for the non-body, un-rotated ray distribution option used in this thesis in a later section.

Radiation Environment

There are several radiation boundary condition options that the user can choose for performing their analysis. They follow a set input and output format that matches the

implemented transport methods. The main environments that will be covered are Solar Particle Events, Galactic Cosmic Rays, Earth Orbit (including trapped protons in Earth's magnetic field and albedo neutrons from Earth's atmosphere), and the Lunar Surface. All of the equations below come from the same OLTARIS reference document and were then verified with additional sources.

Solar Particle Event Spectra

SPE effects in OLTARIS are based on recorded historical events. The recorded energies from these events are used as inputs to find the flux/fluence of the particle moving through the material. The dates used and their corresponding differential formulas are shown below. In all of the equations, $\phi(E)$ is the flux/fluence of the proton particle, *m* is the mass of a proton (about 938 MeV), and *E* is the kinetic energy. LaRC stands for Langley Research Center. The units for all of the SPE spectra are $\frac{protons}{cm^2-AMeV-event}$.

February 1956 Webber, with 100MV rigidity [12,20]:

$$\phi(E) = 1.0 \times 10^7 \left[\frac{E+m}{\sqrt{E(E+2m)}}\right] \exp\left[\frac{239.1-\sqrt{E(E+2m)}}{100}\right] \quad (1)$$

February 1956 LaRC [12,22]:

$$\phi(E) - 6.0 \times 10^7 \exp\left(\frac{10-E}{25}\right) + 9.375 \times 10^5 \exp\left(\frac{100-E}{320}\right) \quad (2)$$

November 1960 [12,22]:

$$\phi(E) = 6.33 \times 10^8 \exp\left(\frac{10-E}{12}\right) + 4.88 \times 10^6 \exp\left(\frac{100-E}{80}\right) \quad (3)$$

August 1972 King [6,12]:

$$\phi(E) = 2.98 \times 10^8 \exp\left(\frac{30-E}{26.5}\right) \quad (4)$$

August 1972 LaRC [12,22]:

$$\phi(E) = 2.2 \times 10^7 \exp\left(\frac{100-E}{30}\right) \quad (5)$$

August 1989 [10,12]:

$$\phi(E) = \frac{8.652 \times 10^{10}}{59.261} \frac{E+m}{\sqrt{E(E+2m)}} \exp\left[\frac{-\sqrt{E(E+2m)}}{59.261}\right] \quad (6)$$

September 1989 [10,12]:

$$\phi(E \leq 10\ MeV) = 1.446 \times 10^8 \frac{E+m}{\sqrt{E(E+2m)}} \exp\left[\frac{-\sqrt{E(E+2m)}}{102.118}\right] \quad (7)$$

In equation 8 below, a smoothing function is added that is the same function for the ≤ 10 MeV range shown above (Eq. 7). When it is a part of this function though it is evaluated at $10\ \text{MeV} < E < 30\ \text{MeV}$ instead of at ≤ 10 MeV.

$$\phi(10\ MeV < E < 30\ MeV) = [-0.0015E^2 + 0.07184E + 0.4304]\, \phi(E \leq 10\ MeV) \quad (8)$$

$$\phi(E \geq 30\ MeV) = \frac{2.034 \times 10^7}{\sqrt{1-\left(\frac{m}{E+m}\right)^2}} \left[\sqrt{\frac{E(E+2m)}{30(30+2m)}}\right]^{-4.5} \quad (9)$$

October 1989 [10,12]:

$$\phi(E) = 6.104 \times 10^8 \left[\frac{E+m}{\sqrt{E(E+2m)}}\right] \exp\left[\frac{-\sqrt{E(E+2m)}}{92.469}\right] \quad (10)$$

Carrington 1859, with 1989 fit [12,17]:

$$\phi(E) = 0.877 \times 0.3841 E^{0.3841-1} \times 4.79 \times 10^{11} \exp(-0.877 E^{0.3841}) \quad (11)$$

Carrington 1859, with 1991 fit [12,17]:

$$\phi(E) = 0.972 \times 0.441 E^{0.441-1} \times 1.47 \times 10^{12} \exp(-0.972 E^{0.441}) \quad (12)$$

Galactic Cosmic Rays

The OLTARIS GCR model is based on a combination of measured data and statistical approximation. Satellite data recorded from 1954 to 1992 combined with the Advanced Composition Explorer satellite data from 1997 to 2002 is used as the basis for the model. This is then combined with the Fokker-Planck equation (Equation 13[7]) to find a fit and solve for the diffusion, convection, and energy loss boundary problem. The diffusion coefficient is then estimated. In cases where there is no measured data, the diffusion coefficient is estimated by using the correlation between the coefficient and the Climax Neutron Monitor data, which showed that there is a 22-year periodic cycle of cosmic ray intensities exhibiting odd-even behavior[12].

$$\frac{1}{r^2}\frac{\partial}{\partial r}(r^2 V_s U) - \frac{1}{3}\left[\frac{1}{r^2}\frac{\partial}{\partial r}(r^2 V_s)\right]\left[\frac{\partial}{\partial T}(\alpha T U)\right] = \frac{1}{r^2}\frac{\partial}{\partial r}\left(r^2 \kappa \frac{\partial U}{\partial r}\right) \quad (13)$$

In Eq. 13, r is the radial position in astronomical units (AU), T is the kinetic energy (MeV/n), $U(r,T)$ is the GCR flux (particles/sr*m^2*s*MeV/n), $V_s(r)$ is the solar wind speed (~400 km/s), $\kappa(r,T)$ is the particle diffusion coefficient tensor, and $\alpha(T) = (T+2T_0)/(T+T_0)$ where T_0 is the GCR particle rest energy[7]. The Fokker-Planck equation is simply used as a statistical model to interpolate and extrapolate the data to get results for all of the cases, including ones with no measured data. It calculates the probability density function of the particle velocity when affected by random forces. The output is all the deceleration parameters that describe the solar cycle level and GCR spectrum at the set dates.

There are currently nine preset GCR scenarios, where the user selects one of the specific dates provided and a mission duration. The dates are 1965 Solar Min, 1970 Solar Max, 1977 Solar Min, 1982 Solar Max, 1987 Solar Min, 1991 Solar Max, 1997 Solar Min, 2001 Solar Max, and 2010 Solar Min. Table 2 shows the deceleration parameters for a previous revision of OLTARIS, where there were 11 preset scenarios as shown below. The documentation has not been updated with new dates since 2010, but the website is constantly updated. The units for the GCR options are $\frac{particles}{cm^2-AMeV-day}$.

Table 2. Example of Deceleration Parameters for Previous Preset GCR Scenarios [12].

Scenario	Deceleration Parameter
1956 Solar Min	401
1959 Solar Max	1986
1965 Solar Min	510
1970 Solar Max	1293
1977 Solar Min (DSNE[3])	474
1982 Solar Max	1924
1987 Solar Min	467
1991 Solar Max	2525
1997 Solar Min	467
2000 Solar Max	1674
2007 Solar Min (predicted)	490

Earth Orbit

The Earth Orbit conditions include options for GCR, trapped protons, and neutron albedo, which can be selected in any combination.

The GCR option for Earth Orbits follows the same model as explained in the previous section, but it is further controlled by a transmission coefficient. This coefficient is scaled for the atmosphere using the Atmospheric Ionization Radiation (AIR) model, which evaluates radiation dose for atmosphere flight [2]. The user can select an orbit starting at a minimum altitude of 200 km. The units are the same as explained above in the GCR environment section.

The trapped protons option also accepts altitudes as low as 200 km, which means that the full effects of the South Atlantic Anomaly are included since this trapped proton region can be as low as about 200 km. The main models for this environment are the AP8MIN and AP8MAX models, which are then interpolated to achieve results. The units for this are $\frac{particles}{cm^2-AMeV-day}$.

The neutron albedo environment is formed from the Earth's atmosphere interacting with GCRs. The model used in OLTARIS is based on data from NASA Langley Research Center's studies between 1965 and 1971. A fit was applied to the data that scaled in and allowed mapping of the neutron environment at all locations and times. The units for neutron albedo are the same as for trapped protons except that the numerator is in neutrons rather than particles (protons): $\frac{\square eutrons}{cm^2-AMeV-day}$.

Lunar Surface

This environment is still a very simplified model because there is no lunar neutron albedo model in OLTARIS yet. The options within this environment are lunar GCR and lunar SPE. The same methods as mentioned before are used for all of the rays in the thickness distribution that point out to space. Any rays that point to the lunar surface are set to have no boundary condition.

Particle Transport

The particle transport module propagates the radiation environment through the geometry being analyzed in OLTARIS. The HZETRN2005 transport model is used for this process, which provides an approximate solution to the Boltzmann transport equation (Equation 14) below. Two approximations, the Continuous Slowing Down Approximation (CSDA) and the "straight ahead" approximation, are used to solve the equation [12].

$$\left[\frac{\partial}{\partial x}-\frac{1}{A_j}\frac{\partial}{\partial E}S_j(E)+\sigma_j(E)\right]\phi_j(x,E)=\sum_k\int_E^\infty dE'\sigma_{k\to j}(E'\to E)\phi_k(x,E') \quad (14)$$

which has the boundary condition $\phi_j(0,E) = f_j(E)$, where $\phi_j(0,E)$ is the flux/fluence of particle *j* at a depth *x* with kinetic energy *E* and f_j is a known function. A_j is the atomic mass number, $S_j(E)$ is the stopping power of ion j with energy *E*, $\sigma_j(E)$ is the total cross section for particle *j* with energy *E*, and $\sigma_{k\to j}(E' \to E)$ is the cross section for interactions where a particle *k* with energy *E'* produce a *j* particle with energy *E*[12].

The two approximations used are based on different assumptions; the CSDA assumes that enough atomic interactions happen per unit path length that it can be considered continuous, while the straight ahead approximation assumes that primary and secondary particles propagate in the same direction.

Equation 14 can be simplified for heavy ions, where *E'* is removed, as shown in Equation 15. This is because a constant velocity approximation is made[12].

$$\left[\frac{\partial}{\partial x} - \frac{1}{A_j}\frac{\partial}{\partial E}S_j(E) + \sigma_j(E)\right]\phi_j(x,E) = \sum_{k>j}\sigma_{k\to j}(E)\phi_k(x,E) \qquad (15)$$

The same approximation cannot be used for light ions, so the equation cannot be simplified. The upper limit for the sum in Eq. 15 can vary; for Eq. 14 the upper limit to the sum is all light particles. This transport solution for light and heavy ions has been shown to be accurate to $O(h^2)$ [12].

In OLTARIS, two transport scenarios are used: a database with three material layers that can be interpolated, and a multi-layer slab with neutron transport. In scenario one, the database generates combinations of the materials for varying thicknesses and densities. If the limit density is exceeded, the grid used is adjusted to accommodate

numbers up to a new limit of 1000 g/cm^2. Scenario two lets the user layer materials in a slab geometry and then the response is calculated for each defined thickness.

Response Functions

OLTARIS has several response functions that have been explained earlier in this write up. More information on them can be seen below.

Dose

The dose is calculated along the particle's path from the energy it deposited. It is defined in Equation 16 below [12].

$$D = \sum_j D_j \tag{16}$$

$$\text{where } D_j = \int_0^\infty dE\, S_j(E)\phi_j(E) + d^*(E)$$

$S_j(E)$ is the stopping power of particle j with energy E, and has units of keV/μm. The $d^*(E)$ term adds the dose of particles that aren't transported through the material. Dose can be reported for tissue or silicon, is output in units of mGy, and can be opened as a Dose Table, which can be interpolated to find the dose at a specific point in the geometry.

LET

OLTARIS uses a numerical approach to define the linear energy transfer throughout all open energy subintervals. This works in spite of the fact that the conversion to LET from particle energy results in LET having some derivatives with respect to energy equal to zero, making it un-integrable. In this way LET spectra can be

plotted. This method, like dose, can be reported for tissue or silicon. LET has units of keV/μm.

Other Functions

As previously mentioned, OLTARIS has the capability of analyzing radiation effects on human tissue representing body within a vehicle geometry. The additional functions are Dose Equivalent, TLD-100, TEPC, and Effective and Organ Averaged Dose Equivalent. These will not be covered since they were not used for this project; however, more information can be found in the documentation on the OLTARIS site or in the references at the end of this document.

Internal OLTARIS Verification

As was explained before, the design for OLTARIS is modular, allowing separate parts to be worked on without interfering with others. Module test cases are run to check the functionality of the individual models while functional tests are run to check that the entire system and the interactions between modules. Changes are made on a test version of the website, and once enough tests have been run and the changes are approved, they are completed on the actual website. All changes made are tracked in a change log.

Furthermore, extensive comparisons occurred between OLTARIS output and measured data from Space Shuttle missions as well as to the ISS TEPC to validate the results. Strict NASA standards for simulation and modeling tools are also met. Details on these tests and standards are in “Independent Verification and Validation Report” and

"OLTARIS Model References," which can be found under the documents tab on the OLTARIS home page [13].

CHAPTER 2

Tool Development

Thickness Distribution File

OLTARIS has built-in thickness distribution options, but they are limited to various types of spheres or slabs. These are extremely helpful for modeling simple systems or performing test runs, but they are less practical when it comes to modeling complex systems that are not one of these two shape types. There is, however, an option for uploading a user-created distribution file in the form of an XML file. This is the method that is used to create a thickness distribution of the P-POD in order to perform radiation analysis. XML stand for "Extensible Markup Language" and is a file extension used for many types of files with varying content [3].

One of the main steps to completing this thesis project, therefore, is the creation of the XML file that can be uploaded onto OLTARIS for radiation analysis. The file contains information on the object's thickness distribution that is found from the CAD file of the object.

Ultimately, this became one if the biggest contributions of this thesis. There are many programs that perform radiation analysis, but they are not easily accessible to the average person or student. There are also programs that perform the ray-tracing analysis required as an input to other analysis methods, but again these are complicated and hard to come by. The process that is explained in the following section is straightforward, easy to use, and accessible to any user. It works in conjunction with OLTARIS for radiation

analysis, but the thickness distribution XML file can be used for any use that it can apply to; it is not limited to OLTARIS or radiation analysis. The code was written because no alternate, open-source methods could be found that performed the necessary ray tracing.

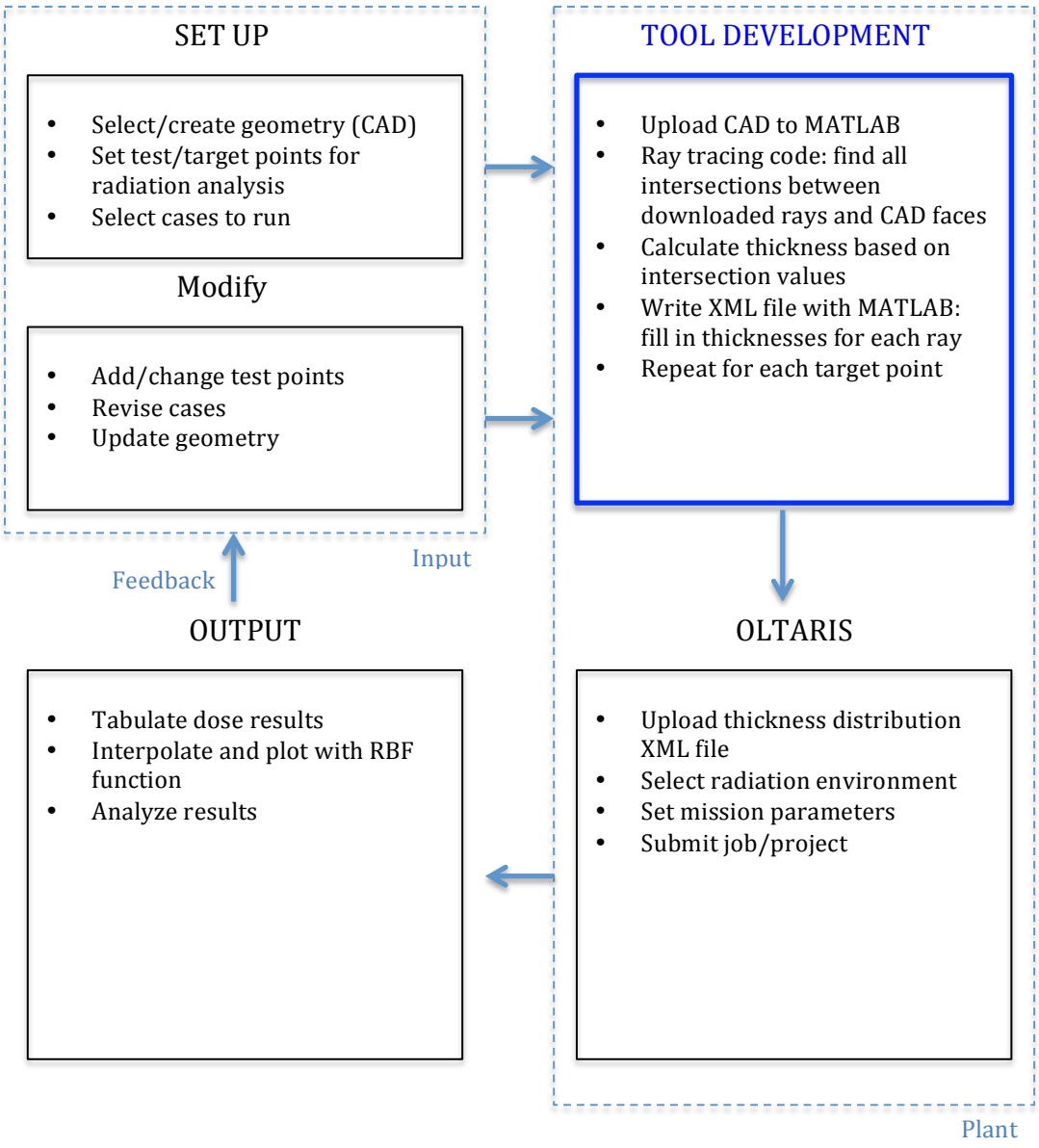

Figure 10. Radiation Analysis Flowchart.

Converting CAD to XML

The first method used to create the XML file involved saving the CAD directly into the XML file format. Many types of CAD software allow for files to be saved in this way by converting the file with a selection from the "Save "As…" dropdown menu. Under the assumption that OLTARIS cannot handle entire assemblies and can only accept "slab" type assemblies of varying thickness, the P-POD CAD file was saved as six separate files, one for each panel. PTC CREO does not save directly to XML, so the files were exported using a downloaded Matlab® add-on called SimMechanics Link. This add-on works with CAD software to export to XML format for use with the SimMechanics tool, allowing for modeling of CAD in SimMechanics [11]. The tool was downloaded only for its Link option that creates the XML files.

After the files were created and the first file upload was attempted, OLTARIS returned an error message stating that the file was incorrect and could not be uploaded because the thickness information could not be pulled out from it. Further research revealed that a specific XML file format is required with certain headings and body information. If the file is set up in any other format it is rejected.

An example of the required format can be seen in Figure 10. Header information is required that details the contents of the file, the creator of the file, the general type of file, etc. This is where information on the materials used in the object are included. The thickness distribution of the object then forms the body of the file. Ray-tracing is used to

find the thickness along a vector, which is then stored. These body sections contain not only the thickness along that vector but also the number identifying which vector is being looked at, its X, Y, and Z directions, the coordinates of the start point of the vector, and the material the vector is going through. In the example in Fig. 11, there are 42 vectors, or rays, used which are provided from the OLTARIS website. Only the first 5 are shown, along with the header and footer information.

```
<?xml version="1.0"?>
<thickness_metafile version_number="1.0">
        <creator name="Chris Sandridge" email="c.a.sandridge@nasa.gov"  />
        <job_bundle job_id="1" job_label="42-ray, 5 g/cm2 Al. Sphere" >
                <analysis_description number_of_zones="1" >
                        <material_table name="generic" type="areal density" units="g/cm2" >
                                <material material_id="1" type_id="1" name="aluminum" />
                                <material material_id="2" type_id="-1" name="Regolith" />
                        </material_table>
                        <thickness_set material_table="generic" type="areal" units="g/cm2"       target_x="0.0"
                          target_y="0.0" target_z="0.0" order="outside_in" >
                                <ray number="1" thk_count="2" xdir="-5.2573100E-01" ydir="0.0000000E+00"
                                  zdir="8.5065100E-01" >
                                        <thk material_id="2" thickness="1.0000" />
                                        <thk material_id="1" thickness="5.0000" />
                                </ray>
                                <ray number="2" thk_count="2" xdir="-3.0901700E-01" ydir="5.0000000E-01"
                                  zdir="8.0901700E-01" >
                                        <thk material_id="2" thickness="1.0000" />
                                        <thk material_id="1" thickness="5.0000" />
                                </ray>
                                <ray number="3" thk_count="2" xdir="0.0000000E+00" ydir="0.0000000E+00"
                                  zdir="1.0000000E+00" >
                                        <thk material_id="2" thickness="1.0000" />
                                        <thk material_id="1" thickness="5.0000" />
                                </ray>
                                <ray number="4" thk_count="2" xdir="0.0000000E+00" ydir="8.5065100E-01"
                                  zdir="5.2573100E-01" >
                                        <thk material_id="2" thickness="1.0000" />
                                        <thk material_id="1" thickness="5.0000" />
                                </ray>
                                <ray number="5" thk_count="2" xdir="3.0901700E-01" ydir="5.0000000E-01"
                                  zdir="8.0901700E-01" >
                                        <thk material_id="2" thickness="1.0000" />
                                        <thk material_id="1" thickness="5.0000" />
                                </ray>
                        </thickness_set>
                </analysis_description>
        </job_bundle>
</thickness_metafile>
```

Figure 11. Example of Partial XML File Format [13].

The footer information closes out the file, similar to how an “end” is used to close out Matlab® functions.

Ray Distributions

As previously mentioned, OLTARIS provides ray distributions that are downloaded and used to create the thickness XML file. There are rotated and unrotated options ranging from as few as 42 rays to as many as 10,000 rays. The rotated options include an input field where certain coordinates are entered prior to the download that align a body inside of the vehicle or object being tested. Since this thesis tested the radiation exposure of electronics rather than human tissue, the unrotated ray distributions were chosen. A visual for the distributions can be seen in Figure 12.

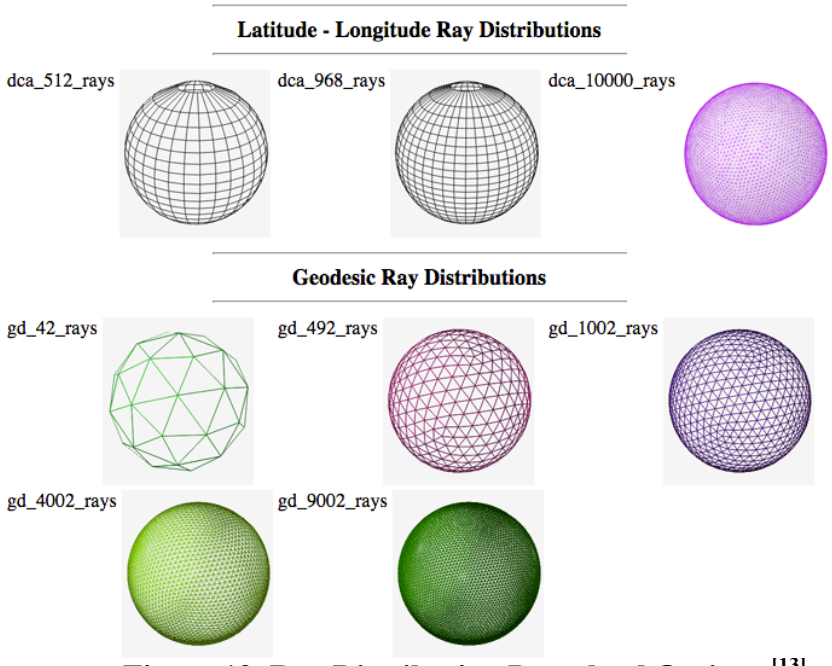

Figure 12. Ray Distribution Download Options [13].

When downloaded and opened, the user sees a text file of X, Y, and Z directions of however many rays were selected.

CAD to Matlab®

In order to perform a ray-tracing of the desired CAD, it is necessary to have the rays and the CAD in one platform. Many companies have in-house ray-tracing programs that take the CAD and the desired ray distribution and output the thicknesses. Since these are not accessible to the average user, a different method had to be developed. The conclusion was that the CAD and ray distribution needed to be read into Matlab, and the analysis would then be performed through a script code.

A code named *cad2mat.m* was downloaded from Matlab® Central[23] that performs the process of reading a CAD file into Matlab®. This function requires the CAD to be saved into an STL file format, which simplifies the geometry into triangles. The triangles are read into Matlab® as a series of faces, vertices, and colors. The colors are only used in the case where the CAD file had different colors set for different parts. Otherwise a default single color is used. Once the face and vertices have been read in, they are stored as variables F, V, and C, and can be used to plot the CAD within Matlab®. It is not necessary to make a plot in order to perform the ray-tracing, but it can be helpful to have a visual. An example figure of the P-POD CAD after being read in can be seen in Figure 13. As can be seen, simple faces use only a few triangles, while corners, chamfered edges, threads, and other complex faces use a large number of triangles.

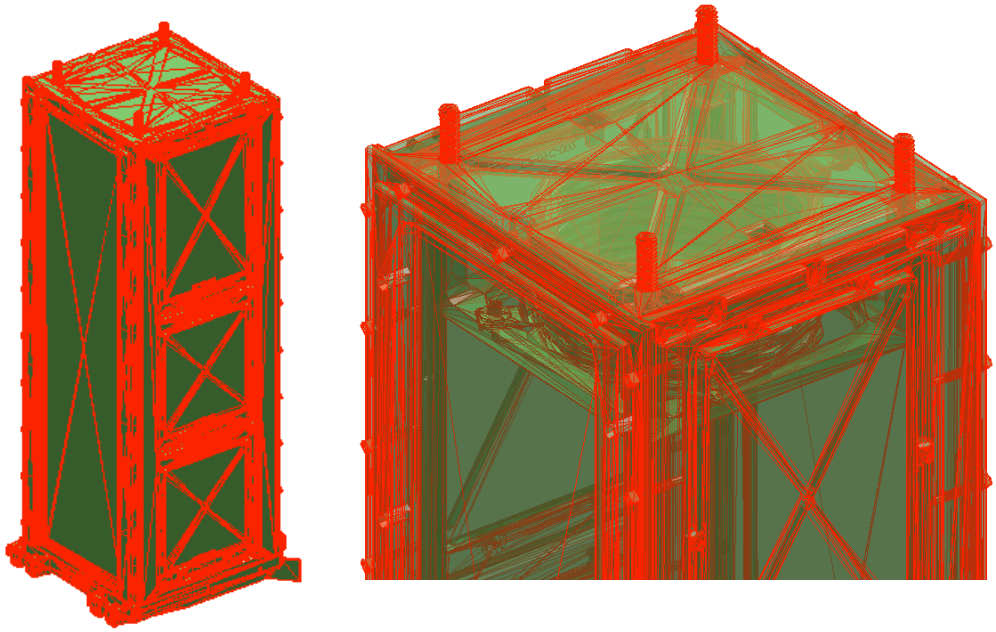

Figure 13. Example Figure of P-POD CAD in Matlab®.

The total amount of triangle faces used to form the P-POD ends up being very high as a result of the mostly complex geometry. The threads in the spring plungers and all of the rounded corners contain hundreds of faces to convert the rounded sections into a series of triangles. This increases the accuracy but also slows down the code. An alternative method for doing this would be to create a simplified model of the P-POD by creating a rectangular box of the same dimensions and similar thickness and using that instead.

Ray-Tracing Code

The script file that calls the *cad2mat.m* function, called *showmethePPOD.m*, saves the variables of the faces and vertices, F and V, into a separate file so that the CAD only has to be read in once but the variables can be loaded and used multiple times. Once

this is done, the ray-tracing process can be done to create the XML thickness distribution file.

A script file *PPODthickdist.m* was written to combine all of the information and separate files and output one XML file. The downloaded ray file is read in and the saved variables file is loaded. A start point is then specified that sets where the ray vectors are radiating out from. This is the "target point", or the point where the radiation levels are being simulated. Each target point is equivalent to one location inside the P-POD.

The code then loops through the ray text file using one ray at a time, checking for an intersection point between that ray's path and each of the triangle faces on the CAD file. Every single face needs to be checked for every ray. The triangle vertices are used to verify that any intersection points found are inside the borders of the face they intersect and are not just in the same plane as the face. There are several algorithms that can be used for this process. Two of them were compared before one was selected for this code.

One of the methods, the Moller-Trumbore (MT) method, uses cross products and dot products to determine if an intersection exists. The other method uses only one cross product and then all dot products for the rest of the math[15]. This alternative method, explained below, was chosen because it is simpler from a mathematical standpoint due to the decrease in cross products. Also, the MT method sometimes resulted in errors from quadrant problems due to the cross products.

The chosen method uses the parametric coordinates of the intersection point on the triangle plane. The parametric plane equation, Equation 17 below[15], is the basis for this.

$$V(s,t) = V_0 + s(V_1 - V_0) + t(V_2 - V_0) = V_0 + s\mathbf{u} + t\mathbf{v} \quad (17)$$

This comes from the three vertices of the triangle, V_0, V_1, and V_2, and real numbers *s* and *t*. The vectors are **u** = V_1-V_0 and **v** = V_2-V_0. Two points along the ray or segment, P_0 and P_1, are used to define the ray. P_I is the same as V(s,t) and is the intersection point. Figure 14 shows the visual representation of the geometry with the labeled points and vectors [15].

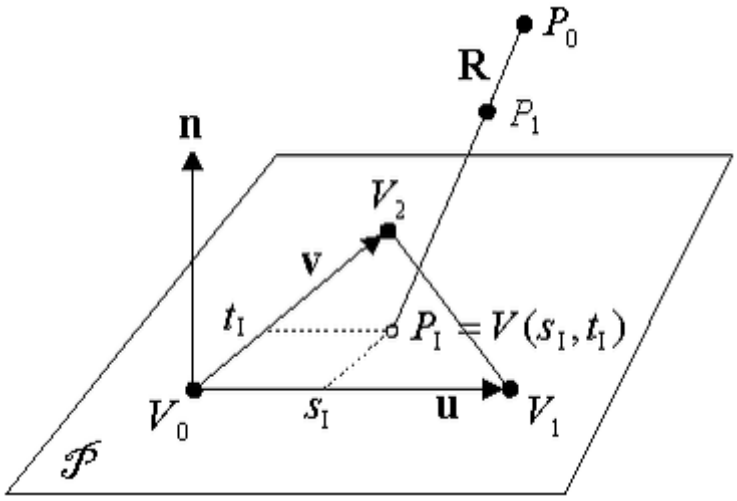

Figure 14. Geometrical Representation of Intersection Point Algorithm [15].

To find *s* and *t*, a series of dot products are used, shown in Equations 18 and 19[15].

$$s_I = \frac{(\mathbf{u}\cdot\mathbf{v})(\mathbf{w}\cdot\mathbf{v}) - (\mathbf{v}\cdot\mathbf{v})(\mathbf{w}\cdot\mathbf{u})}{(\mathbf{u}\cdot\mathbf{v})^2 - (\mathbf{u}\cdot\mathbf{u})(\mathbf{v}\cdot\mathbf{v})} \quad (18)$$

$$t_I = \frac{(\mathbf{u}\cdot\mathbf{v})(\mathbf{w}\cdot\mathbf{u})-(\mathbf{u}\cdot\mathbf{u})(\mathbf{w}\cdot\mathbf{v})}{(\mathbf{u}\cdot\mathbf{v})^2-(\mathbf{u}\cdot\mathbf{u})(\mathbf{v}\cdot\mathbf{v})} \quad (19)$$

After finding the intersection point, three conditions are checked to verify that the point falls within the triangle bounds. These conditions are $s \geq 0$, $t \geq 0$, and $s + t \leq 1$. Furthermore, the intersection point can be determined to be on the edge of the triangle if the "equal to" part of the conditions are true, where $s = 0$, $t = 0$, and $s + t = 1$[15].

Once the intersection points have been found and checked, they are stored in a separate variable. These points are organized in order from closest to farthest from the target point because each ray goes in one side and out the other of a surface. Putting them in order aligns the points so that they are paired off with the first one being the "in" and the next being the "out." The distances between every two points is then calculated. This is the thickness between the parts that the individual ray is going through. This value is then saved in a new variable called "thickness," and the process is repeated for each of the other rays in the downloaded file. A diagram of this process is shown in Figure 15.

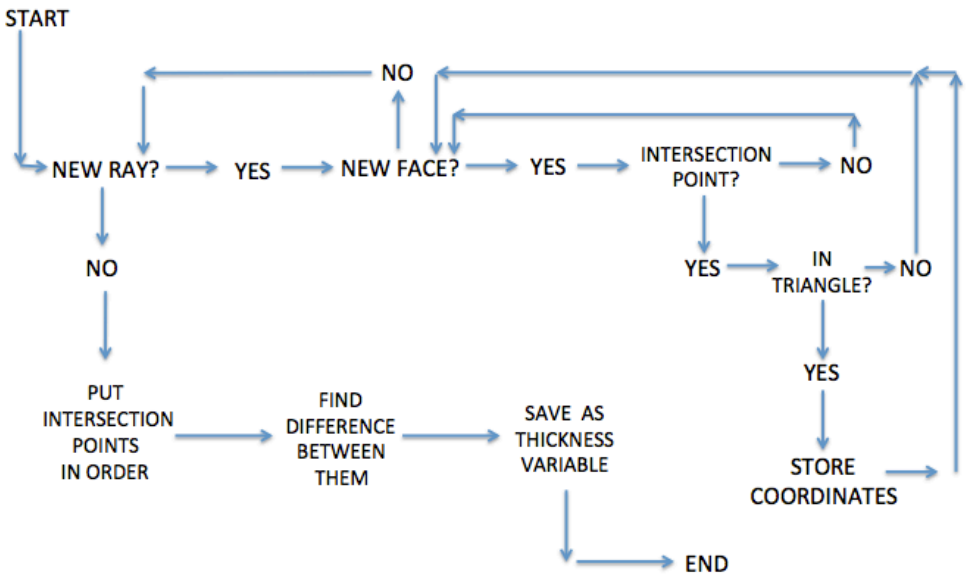

Figure 15. Flow Chart of Ray Tracing Code.

Once all of the thickness values have been calculated, they are converted to the proper units. The *cad2mat.m* file will use whatever units the STL file is saved in. For the P-POD, the units are mm. OLTARIS has several options for units settings, but the chosen option was to use cm. Once the values are converted, a series of *fprintf* statements are used to write the required text and information to a new text file. This text file is saved and is ready to be uploaded to OLTARIS for radiation analysis.

Main Points of Concern

During the creation of the Matlab® script *PPODthickdist.m*, several problems were encountered and are discussed here to avoid similar issues arising in the future.

One issue was the way that the Matlab® script recognized and saved the intersection points. When one ray is checked against all of the faces in the CAD file

triangles, there are multiple intersection points found because several sets of faces are crossed as the ray goes through the object. The problem comes up when the crossing point happens at a triangle vertex or edge. This creates two separate but identical intersection points, making an uneven number of total intersections. These duplicates need to be removed so that putting the intersection points in order does not result in uneven pairs.

Another thing to keep in mind is that the intersection code finds the intersection point assuming that the triangle is an infinite plane and the ray is an infinite line. Once the point is found, it is checked to make sure it falls within the boundaries of the triangle. It is also important to add another limitation so the intersection is in the correct direction for the ray. Otherwise, double thicknesses might be counted since the ray will have intersections in opposite spots of the object when it is extended to an infinite length on both ends rather than one end.

Lastly, there is the occasional occurrence when the code returns an empty matrix of intersections. This can happen if the ray goes through a gap or hole in the CAD. However, this happened when that was not the case. Regardless, both cases are considered to have zero thickness because there is no way to tell the errors apart from the holes. This was not resolved but rather was manually fixed if it occurred.

All of these concerns need to be kept in mind when writing a code to find the thicknesses of a CAD file in Matlab®. In this situation, all three concerns were taken care of through additional coding steps.

CHAPTER 3

Results

OLTARIS Output

Method Verification

After the code creating an XML document was written and corrected, it was necessary to perform a verification test to ensure that the code worked and gave OLTARIS the information to produce accurate results. Otherwise it was possible that the CAD was not being properly read in and converted to the required format.

To check this, a simple test case using two spheres was set up. From the slabs and spheres menu on OLTARIS, a sphere was chosen with a set thickness of 10 cm. This geometry was called "SphereO", and was run at a circular Earth orbit. A sphere of the same thickness was then created using SolidWorks and was named "SphereCAD." It was run on OLTARIS with the same circular Earth orbit as for SphereO. The results are shown in Table 3. The code was found to work correctly since the results between the two spheres were off by significantly less than one percent for all of the results.

Table 3. Sphere Comparison Results.

Environ.	Earth Orbit with altitude of 650 km, inclination of 90 degrees					
Mission	60-day mission duration, starting May 17, 2013 and ending July 16, 2013					
Geometry	**Total Mission Dose (mGy)**	**Rate/Year (mGy)**	**Total GCR Only (mGy)**	**GCR/Year (mGy)**	**Total Trapped Proton and Neutron Albedo Only (mGy)**	**Per Year (mGy)**

SphereO	6.985E+01	4.249E+02	5.028E+00	3.059E+01	6.482E+01	3.943E+02
SphereCAD	6.987E+01	4.250E+02	5.030E+00	3.060E+01	6.484E+01	3.944E+02
% Error	0.0286	0.0235	0.0398	0.0327	0.0309	0.0254

Note that the < 1% error applies specifically to the difference between how OLTARIS converts its native geometries into a thickness distribution file and how the *cad2mat.m* and *PPODthickdist.m* codes converts into a thickness distribution file. As stated in the "Internal OLTARIS Verification" section, comparisons were made between cases created with OLTARIS and actual measurements taken on the ISS and Shuttle missions. The results vary within a wide range for both case types, with OLTARIS showing results between 35%-75% lower than the ISS-TEPC measurements. Although the OLTARIS Shuttle TLD-100 results have a tendency to be closer to the measurements than for the TEPC, they still reached up to 160% difference higher than the measurements. For non-measured orbits (above LEO) the error is approximately 25%.

Although these error values cover a wide range of values above and below measured data, it is important to keep in mind that a lot of variations come into play, such as not having measurements for certain days or cases. Another factor is the OLTARIS assumption that missions start on the 0 hour of the first day and end the last hour of the last day even though inputs allow for partial days. The unpredictability of GCR and SPE occurences and changes in the solar cycle all play a part as well. In spite of the error

percentages, it was deemed after the validation tests that OLTARIS presented the same trends as measured ones and that it was acceptable to use in comparisons [26].

Case Set Up

Prior to running any cases, the P-POD target points need to be selected. Initially, nine points were chosen at three different Z values: three at one end, three in the middle, and three at the bottom. The points were approximately set to be in the middle of the P-POD X-Y plane and at opposite corners, forming a diagonal. It quickly became apparent that more points needed to be included to properly measure the radiation levels, so six more points were added for a final number of 15 different target points on the three cross sections. The location of the three Z values can be seen in Figure 16. Each flat cross section has five points, one in each corner and one in the center.

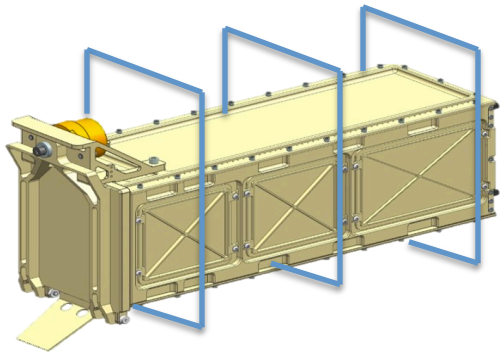

Figure 16. Three Chosen Z Cross Sections.

More points would be beneficial but each point takes a significant amount of computing power. The values of these points can be seen in Table 4. The origin point of the P-POD

as set by the CAD file sits at approximately (-40, 30, 0) because the only symmetrical axis centered around zero is the Z-Axis.

Table 4. P-POD Target Points.

Target Point	X-Value	Y-Value	Z-Value	Target Point	X-Value	Y-Value	Z-Value
1	-75	60	150	**9**	0	0	-140
2	-40	30	150	**10**	-85	-15	150
3	0	0	150	**11**	10	80	150
4	-75	60	0	**12**	-85	-15	0
5	-40	30	0	**13**	10	80	0
6	0	0	0	**14**	-85	-15	-140
7	-75	60	-140	**15**	10	80	-140
8	-40	30	-140				

Radial Basis Function

In order to plot the output from each case run through OLTARIS, the results were put into a Radial Basis Function (RBF). This type of function interpolates the data to get a continuous response from a select few points that are known to be on the solution function. That applies in this situation since only 15 test points are used and not an infinite amount as would otherwise be necessary. The RBF then uses this information and a given X, Y, and Z range to find a solution. The approximation of the solution can change based on the radial function that is chosen, which can take many different forms. Usually the RBF is chosen based on what type of form is believed to be the true solution to the data. The chosen RBF for the P-POD data can be seen in Equation 20,

$$\phi(r) = \sqrt{r^2 + {r_0}^2} \tag{20}$$

where r is the radius found from the training points to the test points and r_0 is a chosen value that is larger than the distance between training points but smaller than the total length scale of the test space. This radial function is for multi-quadratic functions. Although the results for the P-POD are expected to be linear or slightly quadratic, the following test cases show that this RBF is accurate. To show this, a known quadratic equation is used as a comparison to the results from the training points. This was repeated for a known linear equation. The two plots in Figure 17 show that the approximation using the RBF in Eq. 20 is accurate because the plots of real function (green for linear, blue for quadratic) vs. RBF-generated function (colorful) are directly on top of each other. The "X" markers are the location of the training points used in the RBF model.

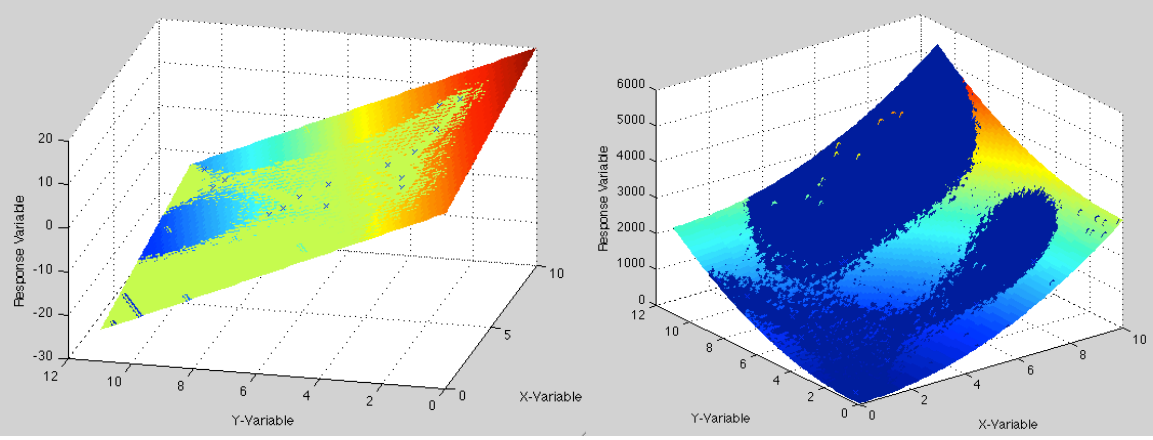

Figure 17. RBF Results for Linear Function (left) and Quadratic Function (right).

Case 1: LEO Orbit

The first case that was run for the P-POD was a circular Earth Orbit trajectory in LEO (Low Earth Orbit) that was designed to be similar to that of a CubeSat in orbit. Although the P-POD does not usually orbit with CubeSats before deploying them, it does

have this capability. Therefore, the radiation levels a P-POD would see if it was in a standard orbit are recorded for use as the comparison for other orbits and scenarios. The mission details and numerical results are in Table 5. Most of the total dose comes from the Total Proton and Neutron Albedo, and a smaller portion is caused by GCRs, as would be expected for a LEO trajectory.

Table 5. Case 1 Results.

Mission: Earth Orbit	Target Point	Total Mission Dose (mGy)	Rate/Year (mGy)	Total GCR Only (mGy)	GCR/Year (mGy)	Total Proton and Neutron Only (mGy)	Per Year (mGy)
Altitude (km)	1	4.126E+02	1.004E+03	1.262E+01	3.072E+01	4.000E+02	9.734E+02
	2	7.418E+02	1.805E+03	1.194E+01	2.906E+01	7.298E+02	1.776E+03
650	3	7.869E+02	1.915E+03	1.197E+01	2.912E+01	7.749E+02	1.886E+03
	4	3.895E+02	9.478E+02	1.272E+01	3.094E+01	3.768E+02	9.168E+02
Inclination (deg)	5	6.260E+02	1.523E+03	1.207E+01	2.938E+01	6.139E+02	1.494E+03
	6	6.785E+02	1.651E+03	1.220E+01	2.969E+01	6.663E+02	1.621E+03
88	7	4.573E+02	1.113E+03	1.249E+01	3.040E+01	4.448E+02	1.082E+03
	8	6.401E+02	1.558E+03	1.209E+01	2.942E+01	6.280E+02	1.528E+03
Duration (days)	9	6.337E+02	1.542E+03	1.213E+01	2.953E+01	6.216E+02	1.513E+03
	10	5.263E+02	1.281E+03	1.232E+01	2.999E+01	5.140E+02	1.251E+03
150	11	4.147E+02	1.009E+03	1.259E+01	3.065E+01	4.021E+02	9.784E+02
	12	6.485E+02	1.578E+03	1.220E+01	2.968E+01	6.363E+02	1.548E+03
Start	13	3.397E+0	8.266E+	1.289E+0	3.137E+	3.268E+0	7.953E+

Date		2	02	1	01	2	02
1/20/2013	14	4.967E+02	1.209E+03	1.243E+01	3.024E+01	4.843E+02	1.178E+03
	15	3.372E+02	8.206E+02	1.290E+01	3.139E+01	3.243E+02	7.892E+02

The total mission dose values were plotted using the RBF function as described above, where the training points are the 15 measured points in the P-POD. Since the P-POD is a three-dimensional object and requires a four-dimensional image to plot it entirely (with the fourth dimension being the radiation values), only cross sections are plotted at the Z-values where the test points where taken. These images show the interpolated value of the radiation levels at every part of the X-Y plane of the P-POD at the three corresponding Z-values. The ranges for the X, Y, and Z axes came from the dimensions of the P-POD in the CAD image file. Figures 18-20 show the results. The color bars on all figures are in mGy, and the magenta “X” markers surrounded by a black circle are the test points.

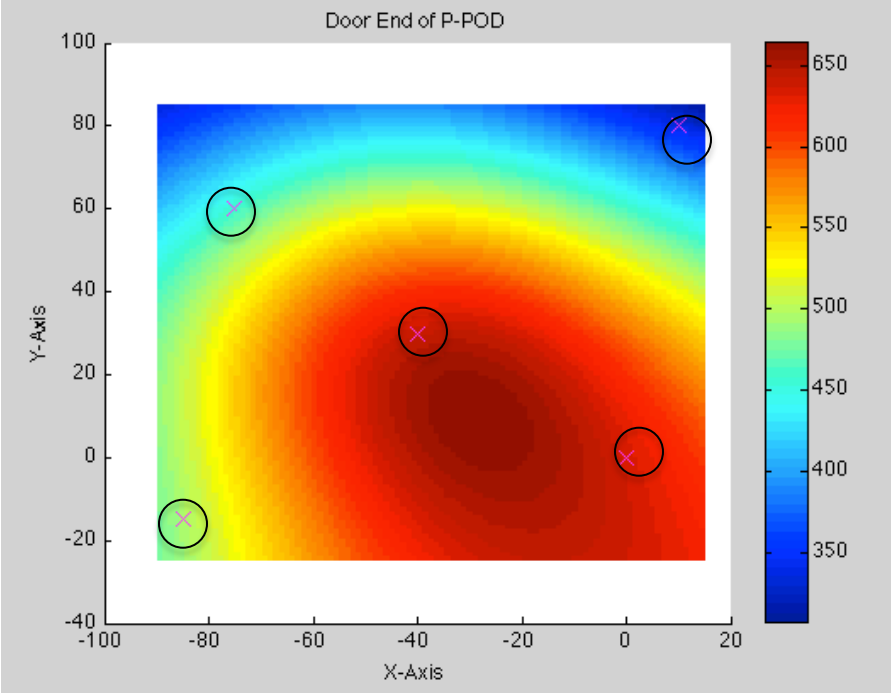

Figure 18. RBF Results for Case 1 at P-POD Door End (mGy, axes in mm).

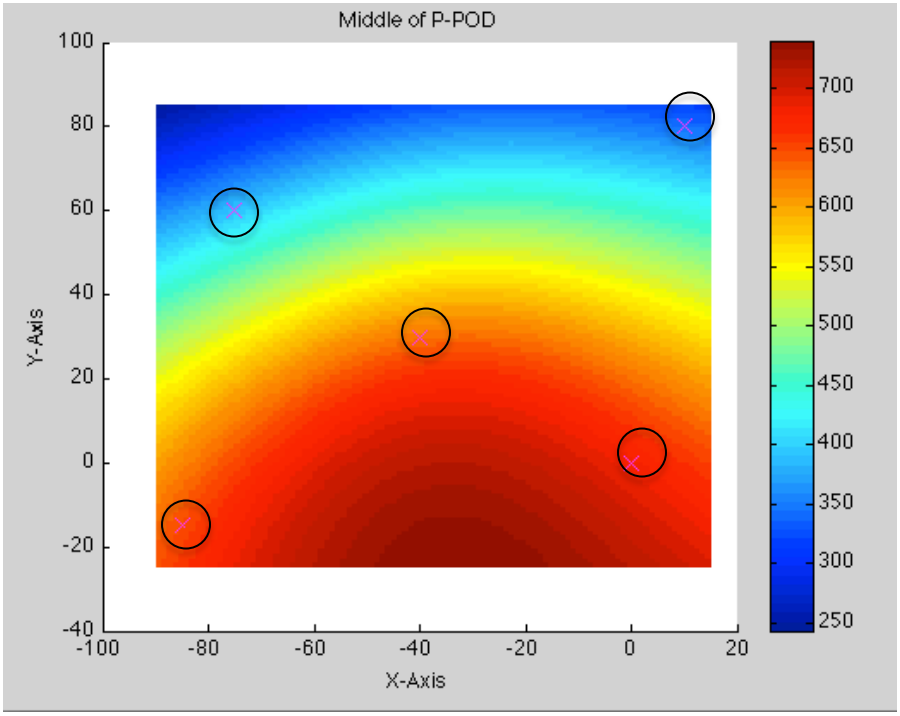

Figure 19. RBF Results for Case 1 at P-POD Middle (mGy, axes in mm).

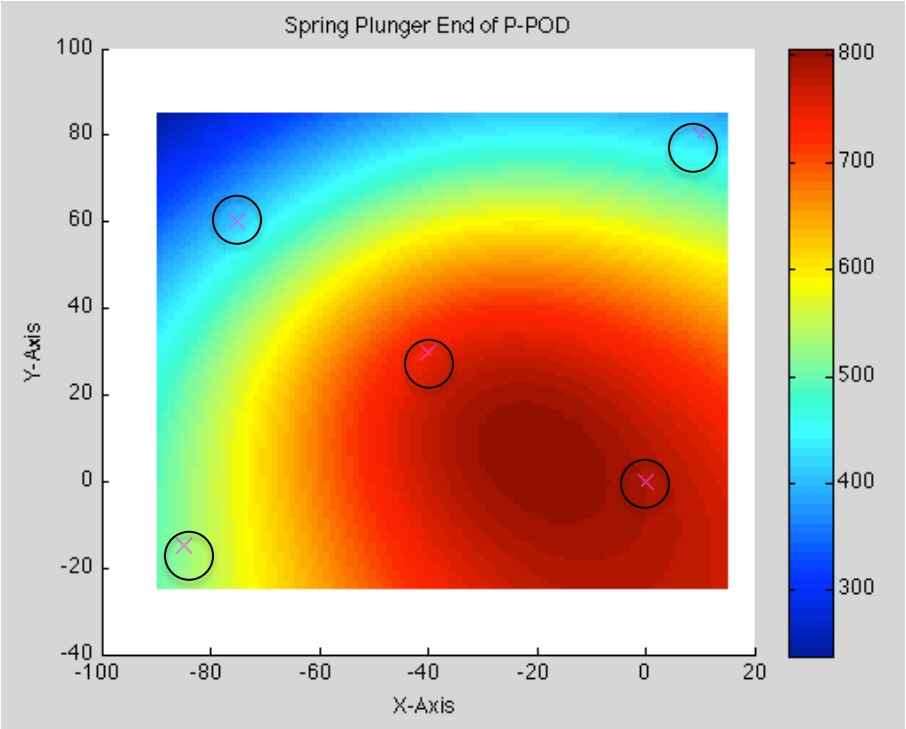

Figure 20. RBF Results for Case 1 at P-POD Spring Plunger End (mGy, axes in mm).

The figures show that the radiation responses of the +Z and -Z areas of the P-POD are similar in shape, with the scale being the main variation. The spring plunger end has higher levels than the other two sections, possibly due to the larger access port covers that are in that region of the P-POD. These covers are thinner than the P-POD wall panels and have a very small gap around the edges on the scale of thousandths of an inch. Still, this is enough to let radiation through. The door end had the narrowest response range and lowest maximum value. This is likely due to a combination of smaller access ports and a thicker door made to withstand the CubeSat deployment loads. The middle section is slightly different than the other two but follows the same overall trend. This is where the

top and bottom come together and meet, so without bigger access ports or a thicker door there, the results pool together and the (-X,-Y) corner does not show a lower radiation level.

The (+X,-Y) corner saw the highest levels in all three sections. This trend was unexpected because the P-POD is symmetric and should see the same levels at a cross-section. It is possible this is an approximation error exaggerated by the RBF function since the actual response is not known, or an error where the CAD model is not as symmetric as it should be. However, the scale in mGy is small so even where there are the biggest differences, they are still relatively small. This does not take away from the overall results and could be improved upon or solved by running many more points in the model.

The levels seen here show that a CubeSat inside the P-POD will generally be safe in this LEO trajectory. The levels are survivable by radiation-hardened electronics as well as COTS (Commercial Off The Shelf) electronics. Table 6 shows common levels that different electronics can survive.

Table 6. Common Electronic Survivability Levels [24] .

	TID	SEL	SEU
Commercial ICs	3-30 krads (Si)	1 - 120 MeV	1 - 120 MeV
Radiation-Enhanced ICs	Customized to Orbit (100 krads (Si) Target)	Customized to Orbit (Up to 120 MeV)	Customized to Orbit (Up to 120 MeV)
Radiation-Hardened ICs	100 krads (Si) Minimum	Up to 120 MeV	Up to 120 MeV

Keep in mind that 1 Gy is equivalent to 100 rads and 1 rad is 6.24×10^7 MeV. Although the table confirms that the P-POD is generally safe in Case 1, there is still a probability of Single Event Upsets that can cause bit flips and other damage.

Case 2: GEO Orbit

The second case was also a circular Earth Orbit but at a higher altitude of 36,000 km. All of the other mission parameters were left the same in order to compare the results based purely on the altitude difference. This simulates the effects of radiation on the P-POD in GEO (Geostationary Earth Orbit), an orbit that is not currently very common for CubeSats. Despite this, it essentially removes all proton and neutron effects in the environment, making it much more similar to what an interplanetary mission would see as it makes its way to another planet. It can also be considered conservative estimate for interplanetary travel because of the added exposure from the Outer Van Allen Belt. The

results in Table 7 show both the dose levels and that the dose is almost completely a result of GCR effects.

Table 7. Case 2 Results.

Mission: Earth Orbit	Target Point	Total Mission Dose (mGy)	Rate/Year (mGy)	Total GCR Only (mGy)	GCR/Year (mGy)	Total Proton and Neutron Only (mGy)	Per Year (mGy)
Altitude (km)	**1**	3.383E+01	8.233E+01	3.383E+01	8.233E+01	1.589E-03	3.866E-03
	2	3.231E+01	7.862E+01	3.231E+01	7.862E+01	1.277E-03	3.107E-03
36,000	**3**	3.235E+01	7.873E+01	3.235E+01	7.872E+01	1.284E-03	3.124E-03
	4	3.403E+01	8.279E+01	3.402E+01	8.279E+01	1.630E-03	3.966E-03
Inclination (deg)	**5**	3.263E+01	7.941E+01	3.263E+01	7.940E+01	1.342E-03	3.265E-03
	6	3.287E+01	7.998E+01	3.287E+01	7.998E+01	1.391E-03	3.386E-03
88	**7**	3.355E+01	8.165E+01	3.355E+01	8.165E+01	1.53E-03	1.020E-03
	8	3.267E+01	7.950E+01	3.267E+01	7.950E+01	1.349E-03	3.282E-03
Duration (days)	**9**	3.276E+01	7.971E+01	3.276E+01	7.971E+01	1.365E-03	3.322E-03
	10	3.318E+01	8.074E+01	3.318E+01	8.074E+01	1.453E-03	3.537E-03
150	**11**	3.378E+01	8.220E+01	3.378E+01	8.219E+01	1.575E-03	3.833E-03
	12	3.287E+01	8.000E+01	3.287E+01	7.999E+01	1.390E-03	3.383E-03
Start Date	**13**	3.436E+01	8.361E+01	3.436E+01	8.361E+01	1.716E-03	4.175E-03
1/20/2013	**14**	3.341E+01	8.130E+01	3.341E+01	8.130E+01	1.499E-03	3.648E-03
	15	3.438E+01	8.365E+01	3.438E+01	8.365E+01	1.721E-03	4.187E-03

The results were again put into the RBF function; the results are shown in Figures 21-23.

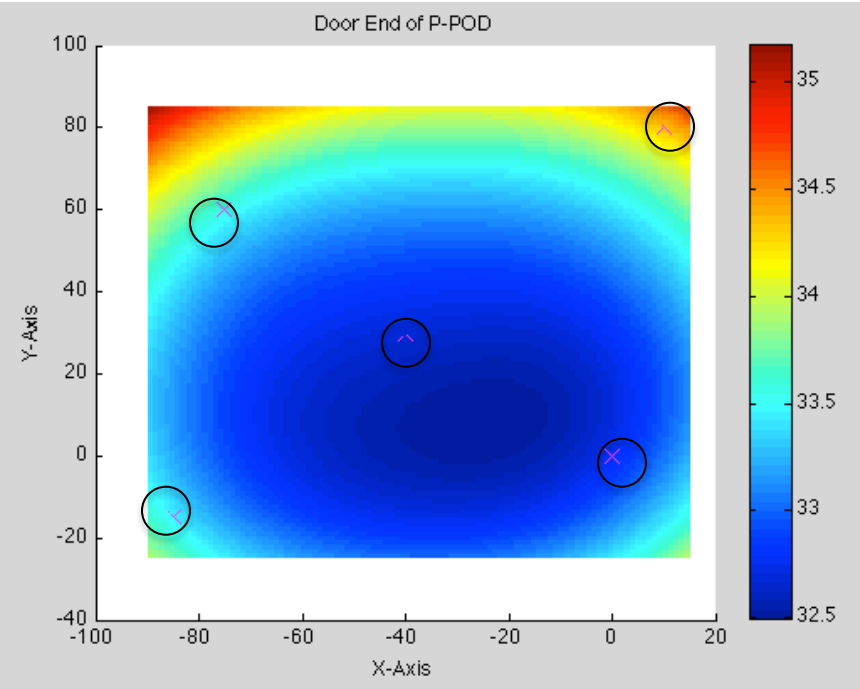

Figure 21. RBF Results for Case 2 at P-POD Door End (mGy, axes in mm).

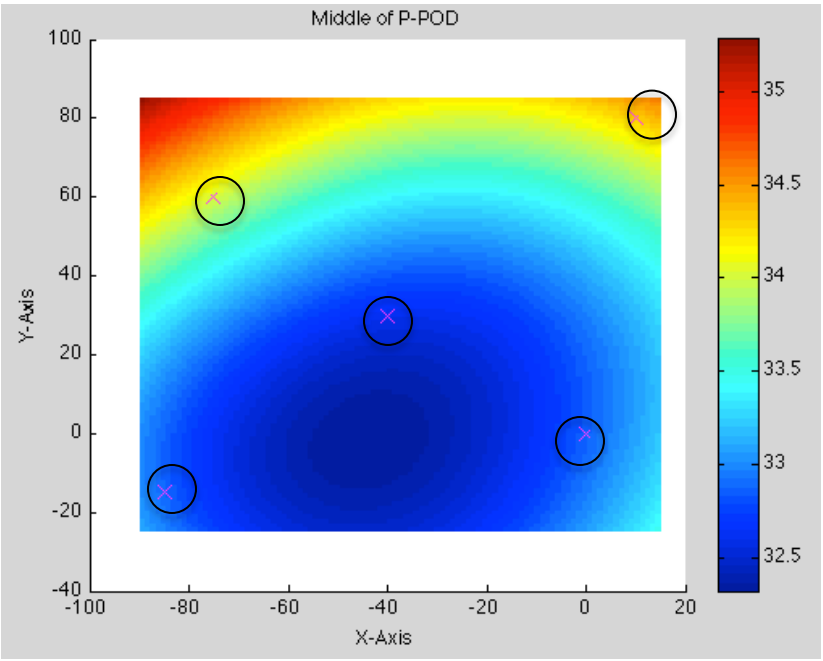

Figure 22. RBF Results for Case 2 at P-POD Middle (mGy, axes in mm).

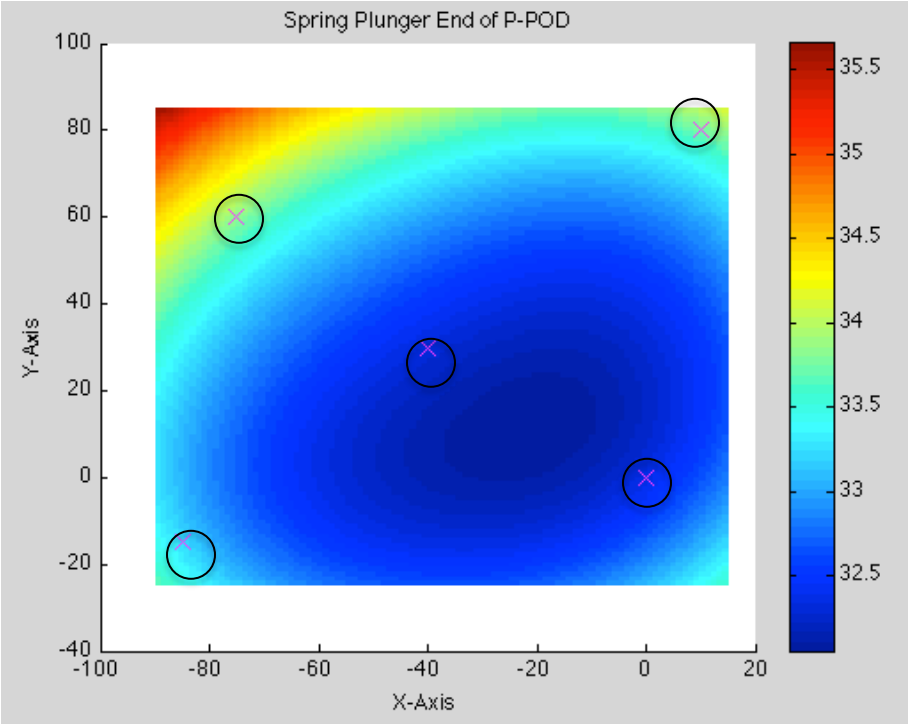

Figure 23. RBF Results for Case 2 at P-POD Spring Plunger End (mGy, axes in mm).

The same trend is seen in these plots as for Case 1, where the scale includes slightly higher levels for the radiation at the spring plunger end. It is a lot less pronounced in this case; there is only an added range of 0.5 mGy at the higher end of the scale. The continued existence of this trend though means that it is actually there and not an error. The smaller range implies that the larger differences seen in LEO are mostly caused by the proton and neutron albedo effects. The results are more symmetric in the X and Y axes than in Case 1, meaning that the error is more likely to come from the RBF method than the P-POD CAD. This is because the lower dose scale results in lower error from interpolation.

However, the main cause for the results being so symmetric in this case is the type of radiation seen. In Case 1, the main type of radiation came from trapped protons and electrons. These can be shielded against through various methods and are therefore more sensitive to changes in thickness. Even small differences in the panels or gaps between parts affect the outcome. In Case 2, the radiation type responsible for almost all of the measured effects is GCRs. These are less easily shielded against since they are very high energy and go through most materials regardless of thickness. The small thickness differences and panel gaps make little to no difference in the radiation levels measured. The images for this case reflect this unique situation by showing that the distribution is even in spite of variations in the thickness across the chosen points. The upper corners, particularly the left one, show higher levels beyond the test point than for the rest of that plane. This is caused by the RBF error mentioned above. Since that upper left test point sees a slightly higher level than the other test points, the RBF interpolates and assumes that the values keep increasing beyond the point, rather than setting the values to be the same. This causes the higher levels "seen" at this corner even though the actual values are within 1 or 2 mGy of the rest of the panel. Because the results have a much smaller range, the probability of having a concave up response (lower in the center) instead of a concave down (higher in the center) increases. The RBF could just as easily shift its interpolation to have a concave down distribution if the values are slightly different but within the same range.

Overall, the numbers are much lower than for Case 1 because there are fewer effects from the Inner Van Allen Belt and the trapped protons and neutrons and the

mission is shorter than an interplanetary mission would be. Still, this provides a scale for how much radiation can be expected for a set mission duration as well as per year for the same geometry. This eliminates the need for blind assumptions on whether the mission is possible or the satellites will survive. As with Case 1, the likelihood of surviving is very high, but there is always the probability of random SEUs that cause unexpected bit flips or other damage.

Case 3: Europa Mission

The third case run was a Europa mission. In this environment, the user only selects the aspect of the mission they want and a thickness distribution. No specific orbital details are provided. The radiation environment components are trapped electrons and trapped protons, and the only response function is dose. This scenario was chosen because it is a good orbit to explore as a preliminary test for an interplanetary CubeSat mission. This type of orbit would be one where a primary spacecraft is performing a Jovian Tour and a deployer will be attached so that CubeSats also perform the tour post-deployment. Since OLTARIS currently only has geocentric orbit capabilities, an interplanetary trajectory cannot be simulated directly. Running a mission on a Jovian Tour Europa orbit provides a good approximation of the radiation environment that might be seen during transit beyond Earth because Jovian missions are high in scientific value and are in NASA's sights as potential options. The Jovian Tour option was specifically chosen because it allows the spacecraft to experience more of the radiation surrounding Jupiter, making it a "worst case" approach. In the other Europa mission options, the spacecraft spends more time shielded from the radiation particles by the planet's

magnetic field, yielding less extreme results. The output of this case is shown in Table 8. Only trapped protons and neutrons are included as options in the Jovian Tour model.

Table 8. Case 3 Results.

Mission: Europa, Jovian Tour					
Target Point	**1**	**2**	**3**	**4**	**5**
Dose (mGy)	9.249E+06	3.086E+07	3.349E+07	7.934E+06	2.312E+07
Target Point	**6**	**7**	**8**	**9**	**10**
Dose (mGy)	2.657E+07	1.204E+07	2.397E+07	2.343E+07	1.660E+07
Target Point	**11**	**12**	**13**	**14**	**15**
Dose (mGy)	9.189E+06	2.454E+07	5.315E+06	1.452E+07	5.193E+06

The results from the RBF function are shown in Figures 24-26.

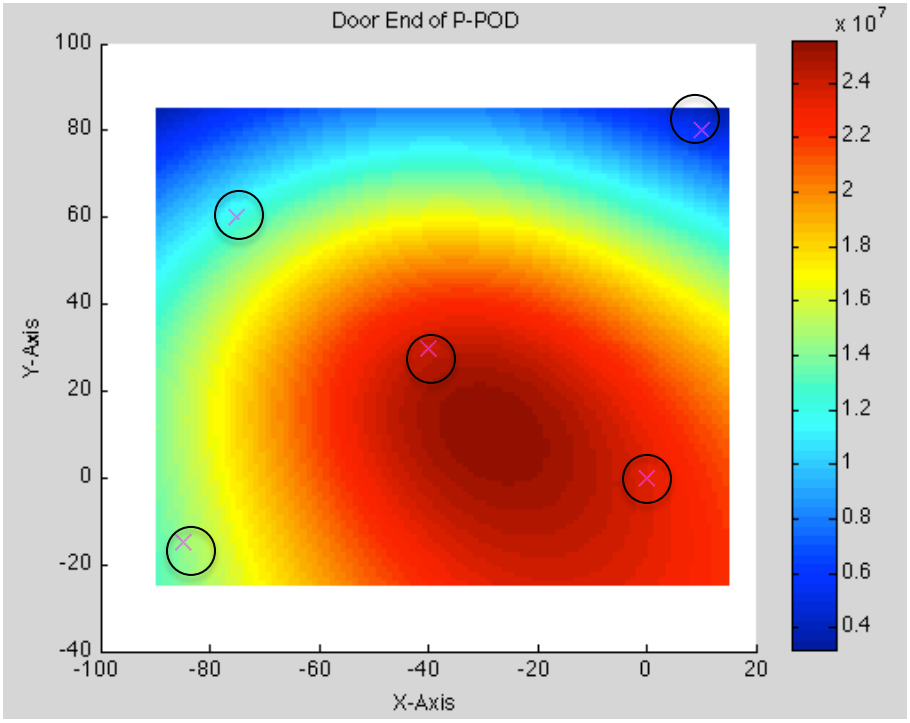

Figure 24. RBF Results for Case 3 at P-POD Door End (mGy, axes in mm).

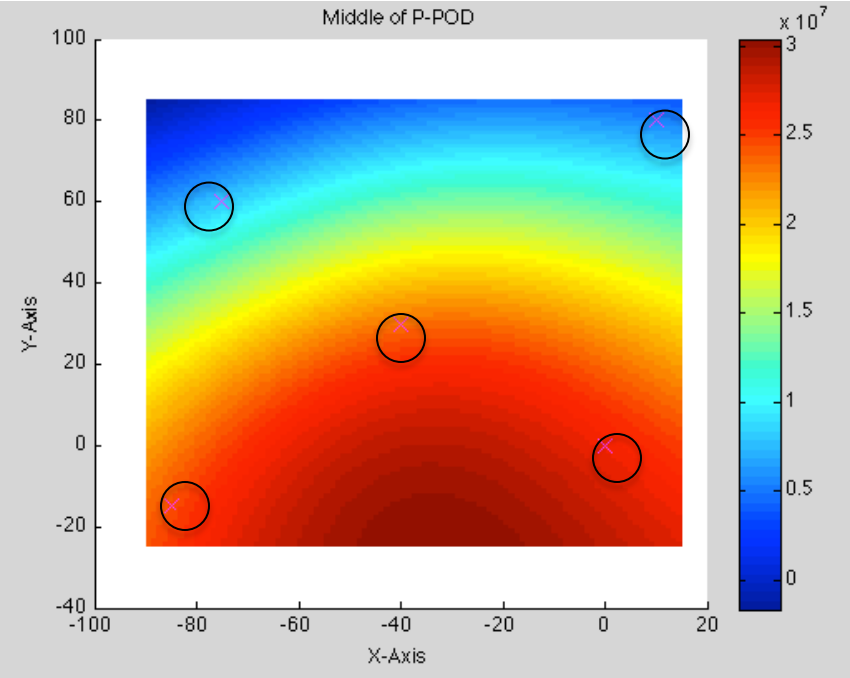

Figure 25. RBF Results for Case 3 at P-POD Middle (mGy, axes in mm).

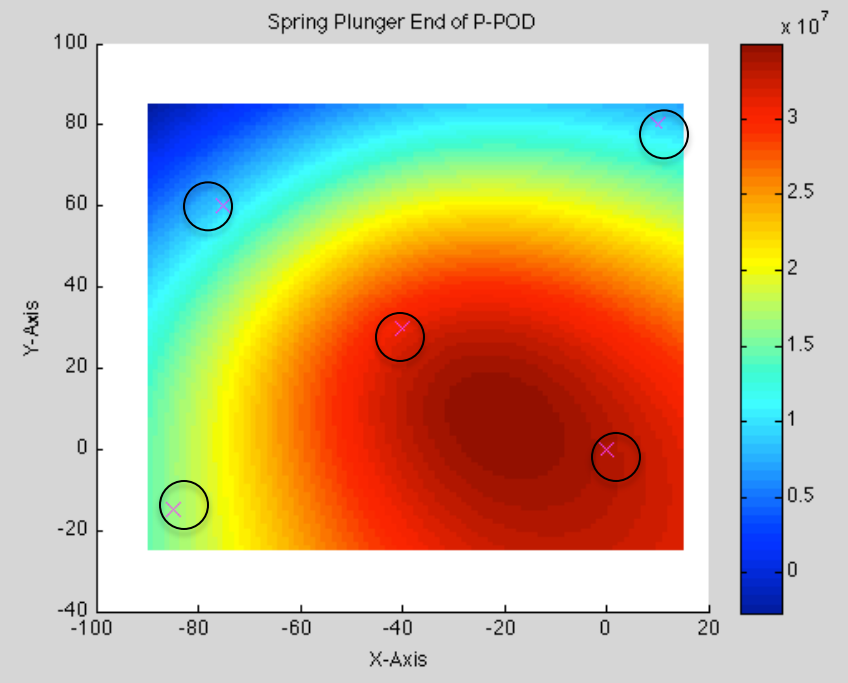

Figure 26. RBF Results for Case 3 at P-POD Spring Plunger End (mGy, axes in mm).

In Case 3, the doses are significantly higher, by several orders of magnitude, than in Case 1 or Case 2. This is due to the higher radiation exposure around Jupiter and the longer mission duration required to perform a Jovian Tour. At these levels, the electronics would not survive the mission. This applies to radiation-hardened electronics as well, which are not commonly used on CubeSats. A significant increase in shielding is required to ensure survival.

The trend in the Z-Axis where the map changes from top to middle to bottom, is consistent with the other cases, verifying the model. The asymmetry in the X and Y axes shows up again due to the large scale range resulting in higher interpolation error from the RBF.

Since these levels were so high, two additional cases were added to see where the line is crossed between not enough shielding and enough (or too much) shielding. A simple multiplication factor was added to the measured P-POD thickness. These extra test cases are explained in the next two sections.

Case 4: Europa Mission 2

The fourth case run was a second Europa mission. The results from the first Europa-Jovian Tour case showed, as expected, that the current P-POD standard is not designed to withstand the radiation levels surrounding Jupiter. To see how the design needs to change, the second Europa-Jovian Tour case was tested with all thicknesses set to be twice as much as the original thicknesses measured from the P-POD. The output of

this case is shown in Table 9. Again, only trapped protons and neutrons are included as options in the Jovian Tour model.

Table 9. Case 4 Results.

Mission: Europa, Jovian Tour					
Target Point	**1**	**2**	**3**	**4**	**5**
Dose (mGy)	4.807E+06	1.887E+07	2.082E+07	3.996E+06	1.366E+07
Target Point	**6**	**7**	**8**	**9**	**10**
Dose (mGy)	1.632E+07	6.305E+06	1.461E+07	1.425E+07	9.506E+06
Target Point	**11**	**12**	**13**	**14**	**15**
Dose (mGy)	4.768E+06	1.491E+07	2.333E+06	8.248E+06	2.251E+06

The results from the RBF function are shown in Figures 27-29.

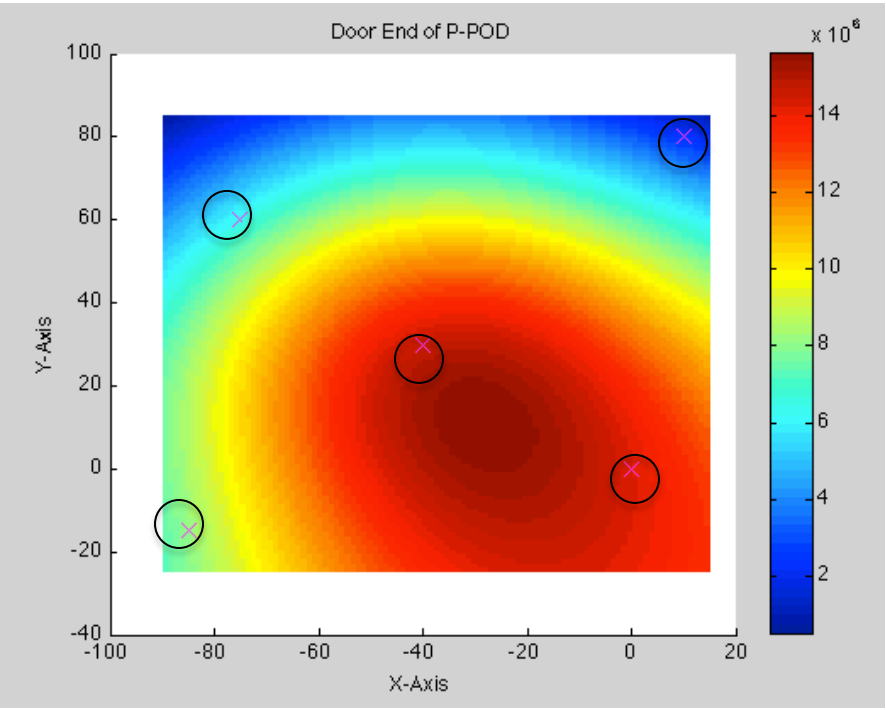

Figure 27. RBF Results for Case 4 at P-POD Door End (mGy, axes in mm).

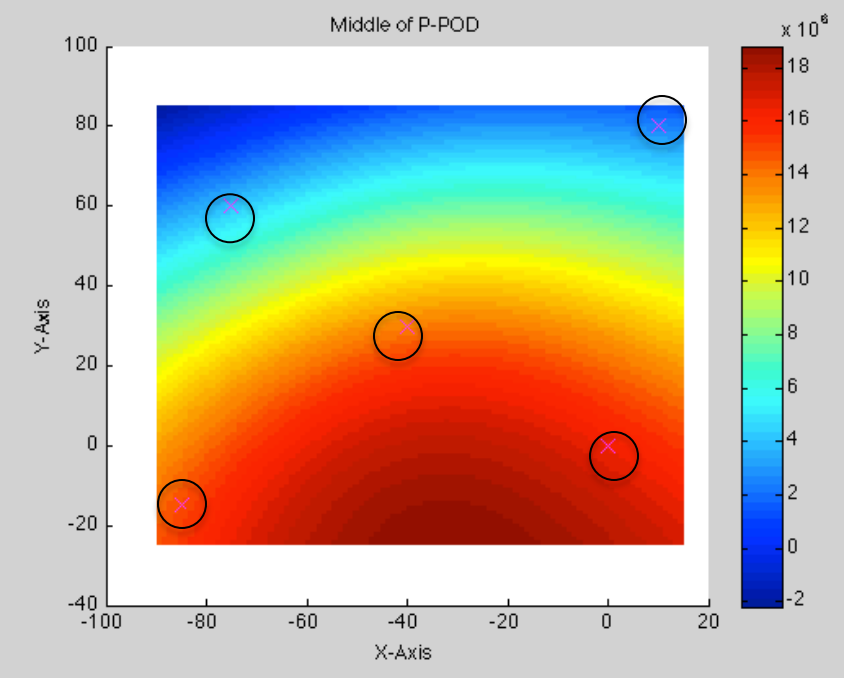

Figure 28. RBF Results for Case 4 at P-POD Middle (mGy, axes in mm).

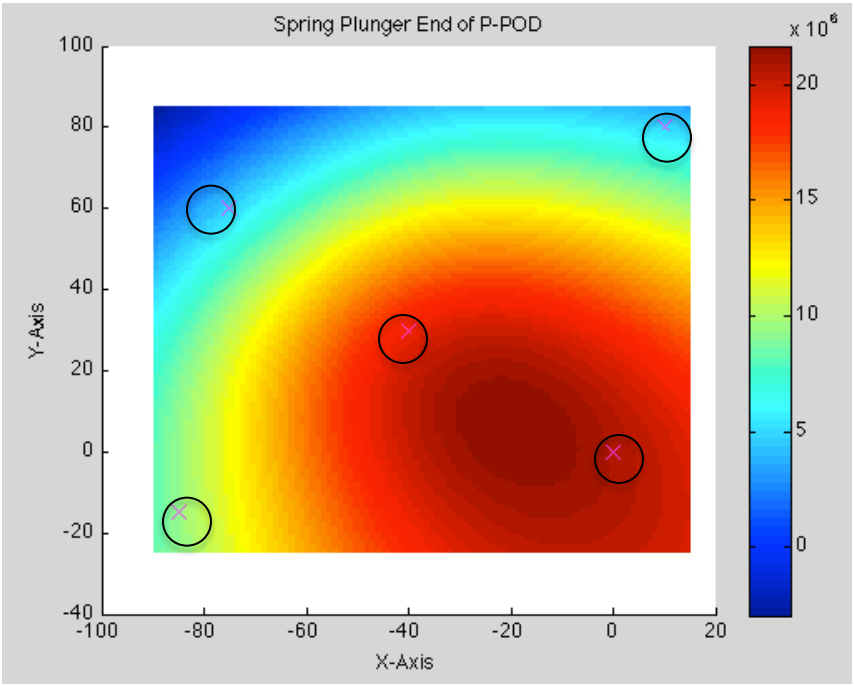

Figure 29. RBF Results for Case 4 at P-POD Spring Plunger End (mGy, axes in mm).

Although the numbers decreased slightly, the order of magnitude stayed the same as in the first Europa-Jovian Tour case. This was not surprising since those levels were so high at 10^6 and 10^7 mGy that doubling a small thickness would increase the shielding at too small of a rate relative to the radiation being seen. The next step taken was more extreme and is discussed below.

Case 5: Europa Mission 3

A final, fifth Europa mission case was run to demonstrate the extremity of the change required to make a dent in the measured radiation dose. The multiplication factor on the thicknesses was changed from two to 100 to force a drastic change in the measured dose levels. The output of this case is shown in Table 10.

Table 10. Case 5 Results.

Mission: Europa, Jovian Tour					
Target Point	**1**	**2**	**3**	**4**	**5**
Dose (mGy)	6.386E+03	9.315E+04	1.533E+05	5.396E+03	3.789E+04
Target Point	**6**	**7**	**8**	**9**	**10**
Dose (mGy)	1.185E+05	1.177E+04	5.852E+04	6.966E+04	2.233E+04
Target Point	**11**	**12**	**13**	**14**	**15**
Dose (mGy)	5.494E+03	8.901E+04	1.033E+03	2.954E+04	9.223E+02

The results from the RBF function are shown in Figures 30-32.

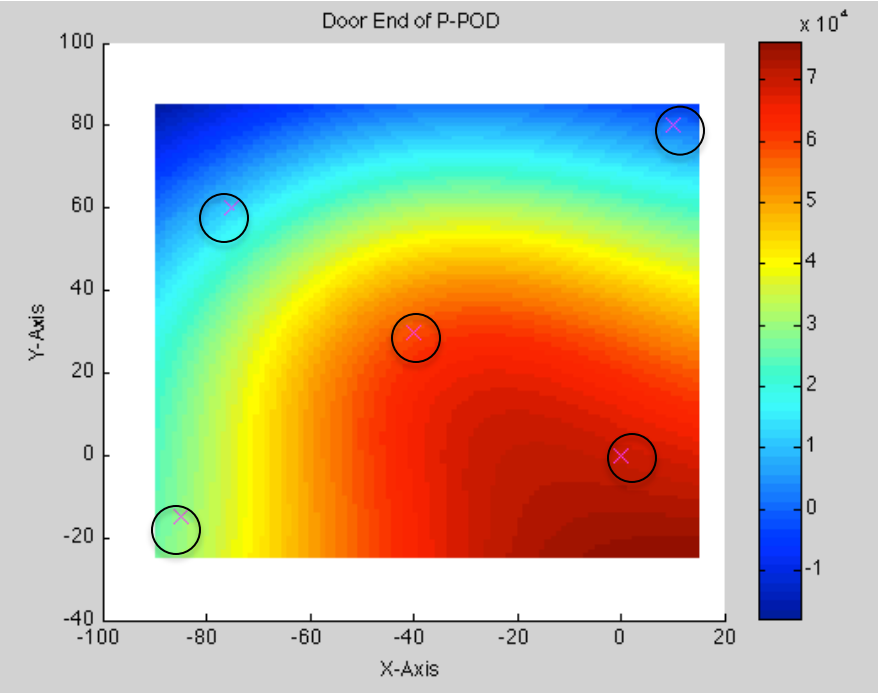

Figure 30. RBF Results for Case 5 at P-POD Door End (mGy, axes in mm).

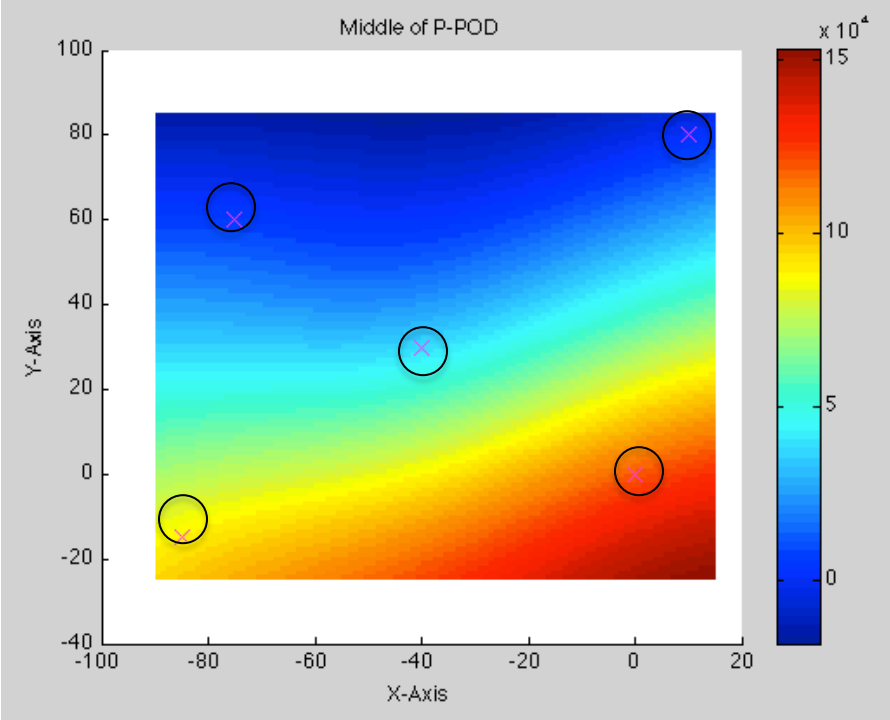

Figure 31. RBF Results for Case 5 at P-POD Middle (mGy, axes in mm).

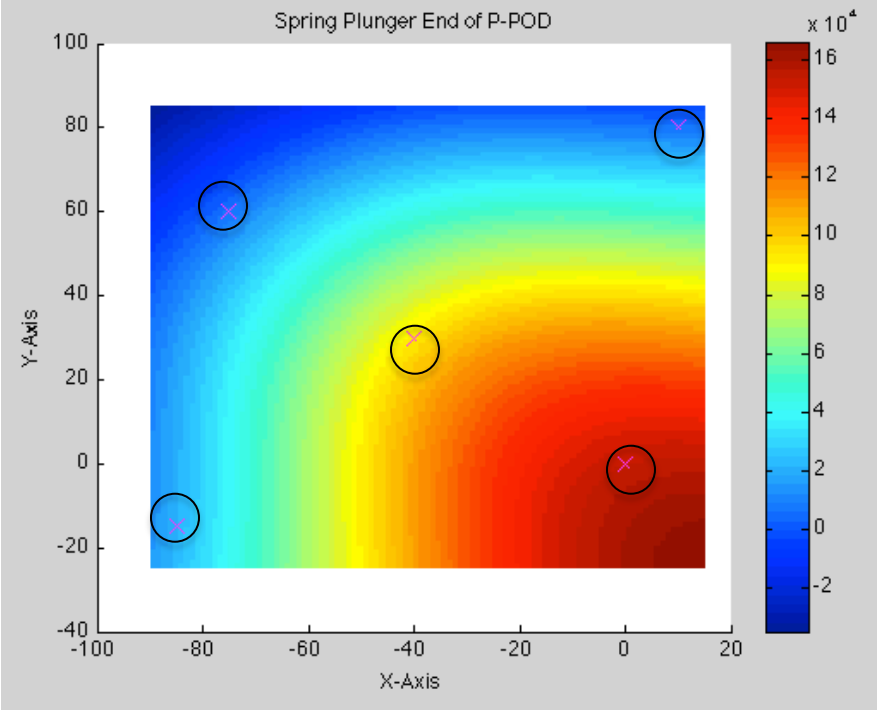

Figure 32. RBF Results for Case 5 at P-POD Spring Plunger End (mGy, axes in mm).

When the thickness is forced to be 100 times its original amount, the order of magnitude decreases to much more reasonable values of 10^3 and 10^4. Although these numbers are not ideal yet, they show the measures that need to be taken to allow survival of a CubeSat around Jupiter. Several things need to be considered along with these results, though. First, increasing the thickness of the P-POD by 100 times its original amount is not a feasible task if the CubeSat and P-POD standards are to remain close to what they currently are to maintain their accessibility and relatively low cost. A five foot thick P-POD wall changes the scope of the spacecraft and no longer allows it to count as part of the picosatellite class. It also does not allow CubeSat missions to be secondary missions. The changes that would make an interplanetary Jovian mission more realistic

require a combination of things such as small thickness increases combined with changes in the P-POD material. Aluminum could be switched out for titanium or other hardier materials. Blankets and coatings, or an additional external case can be added as well. Analysis needs to be performed to find the balance between improving the shielding and increasing the size and mass of the deployer.

The second important thing that needs to be considered in light of these results is that a CubeSat is unlikely to go on a full Jovian tour for a mission. Mission lengths tend to be shorter and the scope more limited than something as broad as this. Although that does not change the high radiation levels surrounding Jupiter, it does present the possibility of lower dose results if a realistic CubeSat Jovian mission is designed and tested. As has been previously explained, the current capabilities of OLTARIS limit the options for interplanetary travel. Once it expands its options and allows the user to tailor missions to meet their more specific needs, more accurate analysis can be performed.

This leads to the third main point to consider, which is that the values OLTARIS provides can be off by a large percentage value from actual data measured at that spot. There is no update provided in the documentation for the percent error in a Jovian case, but since it was established that OLTARIS followed the same trends as measurements taken, the results can still be considered as a starting point or "nominal" setting. Also, the OLTARIS results for the LEO and GEO cases showed values in a range similar to what was expected and are known to be survivable. This leads to the assumption that the error on the Jovian mission is on the lower end of the given range.

Conclusions

As interest in interplanetary CubeSat missions increases, so does the need for further research into the radiation shielding required to make those missions feasible. No thorough analysis has been performed on Cal Poly's Poly-Picosatellite Orbital Deployer (P-POD) to see where its shielding limits lie. Used to take CubeSats to mostly LEO orbits, it is not known if it can withstand a longer journey before CubeSat deployment at another planet. A preliminary interplanetary deployer, the PDSD, was designed to be the next step after the P-POD, but is very similar and has almost the same panel thickness shielding.

This thesis took the established P-POD design and created a code to export the geometry into NASA's open source tool OLTARIS (On-Line Tool for the Assessment of Radiation in Space) to perform analysis at GEO as well as in a Jovian Tour orbit. The tool created can be applied for ray tracing of any geometry at various mission scenarios. While other tools of this type exist, many are internal to companies and owners and not easily available to the average user. This code is open to any user and can be used, as previously mentioned, in conjunction with NASA's OLTARIS program, or with any other radiation analysis tool the user may have access to.

Using the OLTARIS selections available, the environments were set up and tested, after which the resulting output was compared to the acceptable levels of exposure for both radiation-hardened electronics as well as commercial off-the-shelf electronics. The latter option is the one most commonly used for CubeSat missions.

The results seen were as expected, with lower, survivable doses near Earth and higher, fatal doses around Jupiter. There is a balance between the two cases used for interplanetary simulation: the GEO trajectory is conservative in its numbers and shows low doses, while the Jovian Tour trajectory shows high doses. Even if the Jovian Tour is overestimated, the end result is that more shielding and new designs need to be used to improve the current P-POD model in order to survive an interplanetary mission. This also applies to the PDSD design because it currently has wall panel thicknesses that are only slightly thicker than the P-POD. As the Europa-Jovian Tour cases showed, even one hundred times the P-POD thickness is not enough. An improved deployer design will be required, but now that there are approximate numbers to use in the calculations, the new design will be better guided and not based on semi-blind assumptions. The tools are also now available to properly aid in design.

The method developed to create a thickness distribution file for radiation analysis has already been applicable in work outside of this thesis. The Cal Poly Aerospace Senior Design class used it to perform the radiation survivability study of their main spacecraft. They received positive feedback on their results from members of industry, further validating the concept behind this method.

The code used in this thesis is available through the Cal Poly Aerospace Engineering Department.

Future Work

There are several ways in which this thesis can be developed further. One of the main things for further analysis can be to use more than 15 points. This number was chosen based on its coverage of the main sections of the P-POD, but a more accurate map can be created with more points, reducing error from interpolation. Although the overall dose levels won't change, the specific location of each dose value will be more accurate.

Another step is to use the PDSD geometry itself to perform analysis. Although the results are expected to be very similar to the P-POD results, slight variations could be discovered. This would require re-evaluating where the test points should be located and how many need to be used since the structure is larger. Alternatively, the PDSD design could be modified to include thicker wall panels or a combination of shielding materials before using it to perform analysis. This would skip a redundant step and advance the project faster. Analysis would need to be performed to compare the options of increased shielding weighed against the likely increase in total mass.

Lastly, there is a lot of room for improvement of the thickness distribution code. Items such as mated parts are ignored, but they can cause some problems with how the intersection points are found. Currently, a catch is written into the code to overwrite any errors from scenarios like this, but it does not fix the problem. The entire code can also be streamlined further to speed up the process and reduce the run time.

REFERENCES

[1] “Cal Poly CubeSat Program.” N.p., n.d. Web. 1 June 2015. < http://cubesat.org/>.

[2] De Angelis, G. “A New Dynamical Atmospheric Ionizing Radiation (Air) Model for Epidemiological Studies,” *NASA Langley Research Center.*

[3] Fisher, T. *XML File (What It Is & How To Open One).* Web. 1 June 2015. <http://pcsupport.about.com/od/fileextensions/f/xmlfile.htm>.

[4] Gleber, M. "The Difference Between Flares and CMEs." *NASA*. Ed. Holly Zell. NASA Goddard, 21 Sept. 2014. Web. 1 June 2015. <http://www.nasa.gov/content/goddard/the-difference-between-flares-and-cmes>

[5] Heinbockel, J.H., Slaba, T.C., Blattnig, S.R., Tripathi, R.K., Townsend, L.W., Handler, T., Gabriel, T.A., Pinsky, L.S., Reddell, B., Clowdsley, M.S., Singleterry, R.C., Nor- bury, J.W., Badavi, F.F., Aghara, S.K., “Comparison of the Radiation Transport Codes HZETRN, HETC-HEDS and FLUKA using the February 1956 Webber SPE spectrum,” NASA Technical Paper 2009-215560, 2009.

[6] King,J.H.,“SolarProtonFluencesfor1977-1983 Space Missions,” Journal of Spacecraft and Rockets, Vol. 11, No. 6, pp. 401-408, 1974.

[7] O’Neill,P.M., Golge, S., Slaba, T.C., “Badhwar – O’Neill 2014 Galactic Cosmic Ray Flux Model Description,” NASA Technical Paper 2015-218569, 2015.

[8] Pisacane, V. L. *The Space Environment and Its Effects on Space Systems*. Reston: American Institute of Aeronautics and Astronautics, 2008. Print.

[9] Redd, Nola. "Shift of Earth's Magnetic Field." *Space.com*. 9 Oct. 2013. Web. 1 June 2015. <http://www.space.com/23131-earth-magnetic-field-shift-explained.html>.

[10] Sauer, H.H., Zwickl, R.D., Ness, M.J., “Summary Data for the Solar Energetic Particle Events of August Through December 1989,” Space Environment Laboratory, National Oceanic and Atmospheric Administration, 1990.

[11] "SimMechanics." *MathWorks*. Web. 1 June 2015. <http://www.mathworks.com/products/simmechanics/features.html#importing-cad-models>.

[12] Singleterry, Robert C., et al., “OLTARIS: On-Line Tool for the Assessment of Radiation in Space,” NASA Technical Paper 2010-216722, 2010

[13] Spangler J., Simonsen L., and Sandridge C. "OLTARIS Home Page." *OLTARIS*. NASA Langley, 26 Mar. 2015. Web. 1 June 2015. <https://oltaris.larc.nasa.gov/>.

[14] Spangler J., Simonsen L., and Sandridge C. "OLTARIS User Guide." *OLTARIS*. NASA Langley, 26 Mar. 2015. Web. 1 June 2015. <https://oltaris.larc.nasa.gov/>.

[15] Sunday, D. *Intersections of Rays, Planes and Triangles (3D)*. 2001. Web. 1 June 2015. <http://geomalgorithms.com/a06-_intersect-2.html#intersect3D_RayTriangle()>.

[16] Tandberg-Hanssen, E., and A. Gordon Emslie. *The Physics of Solar Flares*. Cambridge: Cambridge UP, 1988. Print.

[17] Townsend, L.W., Zapp, E.N., Stephens, D.L., Hoff, J.L., "Carrington Flare of 1859 as a Prototypical Worst-Case Solar Energetic Particle Event," IEEE Transactions on Nuclear Science, Vol. 50, No. 6, Dec. 2003.

[18] Tribble, A. C. *The Space Environment: Implications for Spacecraft Design*. Revised and Expanded Edition. Princeton: Princeton UP, 1995. Print.

[19] "Van Allen Probes." *NASA*. NASA, 28 Feb. 2013. Web. 1 June 2015. <http://www.nasa.gov/mission_pages/rbsp/news/third-belt.html>.

[20] Webber, W.R., "An Evaluation of the Radiation Hazard due to Solar-Particle Events," D2- 90469 Aero-Space Div., Boeing Co., 1963.

[21] Wilson, J.W., Tripathi, R., Cucinotta, F., Shinn, J., Badavi, F., Chun, S., Norbury, J.W., Zeitlin, C.J., Heilbronn, L., Miller, J., "NUCFRG2: An Evaluation of the Semi-empirical Nuclear Fragmentation Database," NASA Technical Paper 3533, 1995.

[22] Wilson, J.W., Townsend, L.W., Schimmerling, W., Khandelwal, G.S., Khan, F., Nealy, J.E., Cucinotta, F.A., Simonsen, L.C., Shinn, J.L., Norbury, J.W., "Transport Methods and Interactions for Space Radiations," NASA Reference Publication 1257, 1991.

[23] "CAD2MATDEMO.M." *MathWorks*. Web. 1 June 2015. <http://www.mathworks.com/matlabcentral/fileexchange/3642-cad2matdemo-m>.

[24] Dowd, M., "How Rad Hard Do You Need? The Changing Approach To Space Parts Selection? ," Maxwell Technologies Microelectronics, 2003.

[25] Fox, N. "Coronal Mass Ejections." *NASA*. NASA Goddard. Web. 1 June 2015. <http://pwg.gsfc.nasa.gov/istp/nicky/cme-chase.html>.

[26] Stoffle, N., Zapp, N., "On-Line Tool for Assessing Radiation In Space Verification and Validation Effort Using STS DLOC and ISS TEPC Measurements," *OLTARIS*. JSC Space Radiation Analysis Group, 29 March 2010. Web. 1 June 2015. <https://oltaris.larc.nasa.gov/>.